Structural and Molecular Mechanics Studies on Highly Ruffled Low-Spin (Porphinato)iron(III) Complexes

Orde Q. Munro,*[1a] Helder M. Marques,[1a] Peter G. Debrunner,[1b] K. Mohanrao,[1c] and W. Robert Scheidt*[1c]

Contribution from the Centre for Molecular Design, Department of Chemistry, University of the Witwatersrand, Wits 2050, Johannesburg, South Africa, Department of Physics, University of Illinois, Urbana, Illinois 61801, and the Department of Chemistry and Biochemistry, University of Notre Dame, Notre Dame, Indiana 46556

Received February 14, 1994[⊗]

Abstract: A new molecular mechanics (MM) force field model for six-coordinate low-spin imidazole and pyridine complexes of ferric porphyrins has been used with a modified version of the program MM2(87) to investigate the planar and ruffled conformations of $[Fe(TMP)(L)_2]^+$ complexes, where L = a pyridine or imidazole derivative. All currently available X-ray structures in this class were used to gauge parametrization of the force field, including that of $[Fe(TMP)(1,2\text{-}Me_2Im)_2]ClO_4$, whose preparation, Mössbauer spectrum, and X-ray structure determination are described. $[Fe(TMP)(1,2\text{-}Me_2Im)_2]ClO_4$ has the most ruffled core of any iron(III) porphyrin described to date, with mean absolute core atom displacements C_a, C_b, C_m, and C_{av} of 0.41, 0.28, 0.72, and 0.42 Å, respectively. The average $Fe-N_p$ distance is also the shortest observed at 1.937 Å. The MM-calculated and crystallographically observed structures of $[Fe(TMP)(1,2\text{-}Me_2Im)_2]^+$ both show that the porphyrin core is distorted from ideal D_{2d} symmetry in response to anisotropic distribution of steric bulk in the axial ligands. Our calculations indicate that D_{2d}-ruffling of the porphyrin core hinges on a relative perpendicular orientation for the axial ligands, with the magnitude of distortion increasing with increasing ligand bulk (4(5)-MeHIm < pyridine < 1,2-Me_2Im < BzHIm < 2-MeBzHIm). The MM and crystallographic data therefore demonstrate that ligand−porphyrin nonbonded interactions are the primary determinant of core conformation in *six-coordinate* complexes. Furthermore, the *meso*-mesityl groups of $[Fe(TMP)(L)_2]^+$ derivatives exhibit slightly staggered minimum-energy orientations that become more staggered with increasing axial ligand bulk, providing direct evidence for nonbonded interactions between the ligands and the peripheral substituents. Since counterrotation of a trans pair of mesityl groups in D_{2d}-*ruf* $[Fe(TMP)(2\text{-MeBzHIm})_2]^+$ only scarcely perturbed the minimum-energy orientations of the axial ligands, by inducing slight changes in the symmetry of the core distortion and direct intramolecular contact, ligand−peripheral group interactions control the finer aspects of molecular conformation. In contrast, nonbonded interactions between the peripheral aryl groups and the porphyrin core were the primary determinant of core conformation in *four-coordinate* D_{2d}-*sad* [Fe(*meso*-tetraarylporphyrin)]$^+$ species. The calculated core distortion increased with increasing size of the *meso*-aryl substituents (phenyl ≪ 2,6-dichlorophenyl < mesityl). Crystal data for $[Fe(TMP)(1,2\text{-}Me_2Im)_2]ClO_4 \cdot 0.65C_6H_5Cl \cdot 1.05H_2O$: $a = 14.958(24)$ Å, $b = 21.147(21)$ Å, $c = 20.897(32)$ Å, $\beta = 98.98(12)°$, space group $P2_1/n$, $V = 6529$ Å^3, $Z = 4$, $T = 127$ K, number of observed data = 8473, $R_1 = 0.072$, $R_2 = 0.088$.

Introduction

High-resolution X-ray studies on several heme proteins, such as the tetraheme protein cytochrome c_3,[2] oxidized[3] and reduced[4] tuna cytochrome *c*, cytochrome *c* peroxidase,[5,6] and yeast iso-1-cytochrome *c*,[7] have revealed that the heme group geometry is distorted from ideal D_{4h} symmetry. It has been suggested[8−10] that nonplanar conformations of tetrapyrrole prosthetic groups may play a critical role in modulating their physicochemical properties *in vivo*, and extensive work on model systems and heme proteins has established that the ligands coordinated to the axial sites of the metal ion are a strong determinant of the electronic structure of the chromophore.[11−18] Thus, EPR studies on model heme systems[19−21] and cytochromes exhibiting

⊗ Abstract published in *Advance ACS Abstracts*, December 15, 1994.

(1) (a) The University of the Witwatersrand (e-mail: munro@aurum.chem.wits.ac.za; hmarques@aurum.chem.wits.ac.za). (b) University of Illinois. (c) The University of Notre Dame (e-mail: w.r.scheidt.1@nd.edu).

(2) Higuchi, Y.; Kusunoki, M.; Matsuura, Y.; Yasuoka, N.; Kakudo, M. *J. Mol. Biol.* **1984**, *172*, 109.

(3) Takano, T.; Dickerson, R. E. *J. Mol. Biol.* **1981**, *153*, 95.

(4) Takano, T.; Dickerson, R. E. *J. Mol. Biol.* **1981**, *153*, 79.

(5) Wang, J.; Mauro, J. M.; Edwards, S. L.; Oatley, S. J.; Fishel, L. A.; Ashford, V. A.; Xuong, N.; Kraut, J. *Biochemistry* **1990**, *29*, 7160.

(6) Edwards, S. L.; Poulos, T. L. *J. Biol. Chem.* **1990**, *265*, 2588.

(7) Louie, G. V.; Brayer, G. D. *J. Mol. Biol.* **1990**, *214*, 527.

(8) Eschenmoser, A. *Ann. N.Y. Acad. Sci.* **1986**, *471*, 108.

(9) (a) Shelnutt, J. A.; Medforth, C. J.; Berber, M. D.; Barkigia, K. M.; Smith, K. M. *J. Am. Chem. Soc.* **1991**, *113*, 4077. (b) Senge, M. O.; Medforth, C. J.; Sparks, L. D.; Shelnutt, J. A.; Smith, K. M. *Inorg. Chem.* **1993**, *32*, 1716.

(10) Senge, M. O. *J. Photochem. Photobiol. B: Biol.* **1992**, *16*, 3.

(11) Scheidt, W. R.; Gouterman, M. In *Iron Porphyrins*, Part 1; Lever, A. B. P., Gray, H. B., Eds.; Physical Bioinorganic Chemistry Series; Addison-Wesley: Reading, MA, 1983; p 89.

(12) Palmer, G. In *Iron Porphyrins*, Part 2; Lever, A. B. P., Gray, H. B., Eds.; Physical Bioinorganic Chemistry Series; Addison-Wesley: Reading, MA, 1983; p 43.

(13) Debrunner, P. G. In *Iron Porphyrins*, Part 3; Lever, A. B. P., Gray, H. B., Eds.; Physical Bioinorganic Chemistry Series; VCH Publishers: New York, 1989, p 137.

(14) Mus-Veteau, I.; Dolla, A.; Guerlesquin, F.; Payan, F.; Czjzek, M.; Haser, R.; Bianco, P.; Haladjian, J.; Rapp-Giles, B. J.; Wall, J. D.; Voordouw, G.; Bruschi, M. *J. Biol. Chem.* **1992**, *267*, 16851.

(15) Walker, F. A.; Balke, V. L. *J. Am. Chem. Soc.* **1984**, *106*, 6888.

(16) Gadsby, P. M. A.; Thomson, A. J. *J. Am. Chem. Soc.* **1990**, *112*, 5003.

(17) Quinn, R.; Mercer-Smith, J.; Burstyn, J. N.; Valentine, J. S. *J. Am. Chem. Soc.* **1984**, *106*, 4136.

(18) O'Brien, P.; Sweigart, D. A. *Inorg. Chem.* **1985**, *24*, 1405.

(19) Walker, F. A.; Huynh, B. H.; Scheidt, W. R.; Osvath, S. R. *J. Am. Chem. Soc.* **1986**, *108*, 5288.

0002-7863/95/1517-0935$09.00/0

bishistidine axial ligation, for example cytochrome c_3[22] and the mitochondrial cytochromes b,[23,24] have shown that changes in the relative orientations of the coordinated imidazole ligands cause significant changes in the observed g values for these low-spin complexes. The relative orientations of planar axial ligands may also be determined by ^{1}H NMR spectroscopy since the anisotropy of spin delocalization from the metal to the heme periphery depends on the axial transfer of spin from the ligands to the metal (L → M π donation)[25,26] and the equatorial porphyrin e(π^*)−e(dπ) orbital interaction. This has recently been the focus of several studies on bisimidazole iron porphyrins[26-28] and hemoproteins.[29-31] The EPR and NMR results clearly demonstrate, in conjunction with theoretical calculations,[32] that the distribution of unpaired spin within the dπ orbitals (and hence porphyrin π-MO's) is sensitive to the specific orientations of axially coordinated pyridine and imidazole ligands.

But to what extent does the porphyrin conformation contribute to the electronic structure of the metal ion? Resonance Raman[33-36] and structural[37] studies on metalloporphyrins have clearly revealed that S_4-ruffling of the porphyrin core is characterized by contraction of the M−N_p bonds; consequences of this are possible enhanced σ-donation in the equatorial plane from the porphyrin ligand and stronger porphyrin e(π^*)−e(dπ) orbital overlap with a concomitant increase in M−porphyrin π-bonding. In fact, a series of synthetic "basket-handle" tetraarylporphyrins has recently been used to demonstrate that the electronic and redox behavior of porphyrins and metalloporphyrins may be modulated by controlled conformational changes of the porphyrin core.[38]

If nonplanar prosthetic group conformations are functionally significant, then what combination of intramolecular interactions produces the observed distortion, and what factors determine the extent of core ruffling? There is both structural[39,40] and theoretical[41] evidence to suggest that the ligands coordinated at the axial sites of a metalloporphyrin determine whether the porphyrin adopts a planar or ruffled conformation. Core conformation and axial ligand orientation are therefore interdependent and undoubtedly exert a combined effect on the electronic structure of the metal ion. One of our principal objectives is to identify and systematically examine the factors that control the conformations of heme groups and to understand how they might cooperatively determine the electronic structure of the chromophore and central metal ion.

We have recently demonstrated[42] that, by selective distribution of steric bulk between the axial and equatorial (porphyrin) ligands, strongly ruffled low-spin iron(III) porphyrins may be obtained in the solid state and the conformations locked at low temperature in solution. Thus, while [Fe(TMP)(1-MeIm)$_2$]ClO$_4$ and [Fe(OEP)(4-NMe$_2$Py)$_2$]ClO$_4$[21] have planar porphyrin cores, [Fe(TMP)(4-NMe$_2$Py)$_2$]ClO$_4$, [Fe(TMP)(3-EtPy)$_2$]ClO$_4$, [Fe(TMP)(3-ClPy)$_2$]ClO$_4$, and [Fe(TMP)(4-CNPy)$_2$]ClO$_4$[42] exhibit ruffled cores of near D_{2d} symmetry. D_{2d}-*ruf* and planar (D_{4h}) porphyrin cores are obtained when the axial ligands adopt staggered and eclipsed relative orientations, respectively, with two key factors favoring the former: (i) the planar axial ligands must have considerable steric bulk, and (ii) the porphyrin must carry bulky peripheral substituents that are capable of interacting with the coordinated axial ligands. Normally, when conditions (i) and (ii) are met, the axial ligands rotate about the Fe−N_{ax} bonds until the dihedral angle between the ligand planes is ~90°. This induces strong ruffling in the porphyrin core, which effectively diminishes the contact distances between the ligands and the peripheral groups. Since these two criteria are not met in either [Fe(TMP)(1-MeIm)$_2$]$^+$ or [Fe(OEP)(4-NMe$_2$Py)$_2$]$^+$, both are planar. We[42] have also shown that if the axial ligands are chosen to have a range of basicities, it is possible to progressively shift the ground state electronic configuration of the metal from mainly $(d_{xy})^2(d_{xz},d_{yz})^3$ to predominantly $(d_{xz},d_{yz})^4(d_{xy})^1$, indicating that a combination of electronic and conformational factors may exert an appreciable effect on the character of the metal ion.

Generally, the task of quantifying such steric interactions is not simple, although arguments invoking steric effects are intuitively appealing. We recently reported[41] molecular mechanics calculations on metalloporphyrins, using a modified version of the program MM2,[43] which demonstrated the important roles that the size of the coordinated metal ion, the nature and orientations of the axial ligands, and the orientations of peripheral phenyl groups have on the conformation of the porphyrin core. Buckling of the core in [Fe(porphine)(2-MeHIm)$_2$]$^+$ to produce a *ruf*[39,40] conformation was found to depend on the M−L distance to the staggered pair of axial 2-MeHIm ligands, while the magnitude of D_{2d} ruffling producing a *sad*[39,40] distortion depended on the relative orientations of the *meso*-phenyl groups in [Fe(TPP)]$^+$. Furthermore, only planar

(20) (a) Soltis, M. S.; Strouse, C. E. *J. Am. Chem. Soc.* **1988**, *110*, 2824. (b) Quinn, R.; Valentine, J. S.; Byrn, M. P.; Strouse, C. E. *J. Am. Chem. Soc.* **1987**, *109*, 3301.
(21) Safo, M. K.; Gupta, G. P.; Walker, F. A.; Scheidt, W. R. *J. Am. Chem. Soc.* **1991**, *113*, 5497.
(22) Palmer, G. *Biochem. Soc. Trans.* **1985**, *13*, 548.
(23) Carter, K. R.; T'sai, A.-L.; Palmer, G. *FEBS Lett.* **1981**, *132*. 243.
(24) T'sai, A.-L.; Palmer, G. *Biochim. Biophys. Acta* **1982**, *681*, 484.
(25) Abbreviations: BzHIm, benzimidazole; 3-ClPy, 3-chloropyridine; 4-CNPy, 4-cyanopyridine; 3-EtPy, 3-ethylpyridine; HIm, imidazole; L, ligand in general; M, metal ion; MM, molecular mechanics; 1-MeIm, 1-methylimidazole; 2-MeHIm, 2-methylimidazole; 1,2-Me$_2$Im, 1,2-dimethylimidazole; 2-MeBzHIm, 2-methylbenzimidazole; 4(5)-MeHIm, 4- or 5-methylimidazole (tautomeric); *c*-Mu and *t*-Mu, *cis*- and *trans*-methyl urocanate (methyl 4-imidazoleacrylate), respectively; N_{ax}, coordinated axial ligand nitrogen atom; N_p, porphinato nitrogen; T-2,6-Cl$_2$PP, 5,10,15,20-tetra-2,6-dichlorophenylporphyrin; OETPP, 2,3,7,8,12,13,17,18-octaethyl-5,10,15,20-tetraphenylporphyrin; Py, pyridine; TMP, 5,10,15,20-tetramesitylporphyrin; TPP, 5,10,15,20-tetraphenylporphyrin.
(26) Walker, F. A.; Simonis, U. *J. Am. Chem. Soc.* **1991**, *113*, 8652.
(27) Nakamura, M.; Nakamura, N. *Chem. Lett.* **1991**, 1885.
(28) Nakamura, M. *Chem. Lett.* **1992**, 2423.
(29) La Mar, G. N.; Burns, P. D.; Jackson, J. T.; Smith, K. M.; Langry, K. C.; Strittmatter, P. *J. Biol. Chem.* **1981**, *256*, 6075.
(30) Thanabal, V.; de Ropp, J. S.; La Mar, G. N. *J. Am. Chem. Soc.* **1987**, *109*, 265.
(31) McLachlan, S. J.; La Mar, G. N. *Biochim. Biophys. Acta* **1988**, *957*, 430.
(32) Scheidt, W. R.; Chipman, D. M. *J. Am. Chem. Soc.* **1986**, *108*, 1163.
(33) Choi, S.; Spiro, T. G.; Langry, K. C.; Smith, K. M.; Budd, L. D.; La Mar, G. N. *J. Am. Chem. Soc.* **1982**, *104*, 4345.
(34) Spiro, T. G. In *Iron Porphyrins*, Part 2; Lever, A. B. P., Gray, H. B., Eds.; Physical Bioinorganic Chemistry Series; Addison-Wesley: Reading, MA, 1983, p 89.
(35) Piffat, C.; Melamed, D.; Spiro, T. G. *J. Phys. Chem.* **1993**, *97*, 7441.
(36) Sparks, L. D.; Medforth, C. J.; Park, M.-S.; Chamberlain, J. R.; Ondrias, M. R.; Senge, M. O.; Smith, K. M.; Shelnutt, J. A. *J. Am. Chem. Soc.* **1993**, *115*, 581.
(37) Scheidt, W. R.; Reed, C. A. *Chem. Rev.* **1981**, *81*, 543.
(38) Ravikanth, M.; Reddy, D.; Misra, A.; Chandrashekar, T. K. *J. Chem. Soc., Dalton. Trans.* **1993**, 1137.

(39) *Ruf* and *sad* are the two D_{2d}-ruffled core conformations;[40] an ideal *ruf* conformation has alternate up-down displacements of the methine or *meso* carbon atoms and rotation of the pyrrole rings about the M−N bonds, while the ideal *sad* conformation has the methine carbons in-plane but equivalent up-down displacements of alternate pairs of pyrrole β-carbon atoms. The symmetry elements in the two conformations are rotated by 45° around the heme normal.

(40) Scheidt, W. R.; Lee, Y. J. *Struct. Bonding* **1987**, *64*, 1.
(41) Munro, O. Q.; Bradley, J. C.; Hancock, R. D.; Marques, H. M.; Marsicano, F.; Wade, P. W. *J. Am. Chem. Soc.* **1992**, *114*, 7218.
(42) Safo, M. K.; Gupta, G. P.; Watson, C. T.; Simonis, U.; Walker, F. A.; Scheidt, W. R. *J. Am. Chem. Soc.* **1992**, *114*, 7066.
(43) (a) Allinger, N. L. *J. Am. Chem. Soc.* **1977**, *99*, 8127. (b) Allinger, N. L.; Yuh, Y. MM2(87). Distributed to academic users by QCPE, under special agreement with Molecular Design Ltd., San Leandro, CA.

core conformations were found, in agreement with crystallographic data,[20b,44,45] for complexes having *eclipsed*, or near-eclipsed, imidazole or pyridine ligands.

The combined application of X-ray crystallography and molecular mechanics methods to the study of the structural and conformational properties of metalloporphyrins, and other biomimetic macrocycles, currently represents a profoundly useful approach, but this had to await the development and parametrization of force fields suitable for transition metal complexes,[9,36,46] even though reliable force fields have been available for organic compounds for some time.[43a,47-49] One of the advantages of using molecular mechanics calculations is that in addition to structural parameters, the components of the total strain energy of the molecule may be extracted, and therefore correlated, as a function of various applied perturbations. Such experiments then permit quantification of the intramolecular steric interactions contributing to the conformational architecture of the molecule. In this article we report on the crystal and molecular structure of the most strongly ruffled iron(III) porphyrin to date, $[Fe(TMP)(1,2\text{-}Me_2Im)_2]ClO_4$, and present part of a new molecular mechanics force field for low-spin bisimidazole and bispyridine complexes of ferric porphyrinates. The force field has been used to calculate the conformational properties of some four-coordinate *meso*-tetraaryl-substituted iron porphyrins and low-spin bisimidazole and bispyridine complexes of $[Fe(TMP)]^+$. Specifically, we have attempted to define the factors controlling (i) the orientation of the axial ligands, (ii) the orientation of the peripheral *meso* substituents, and (iii) the extent and type of distortion of the porphyrin core.

Experimental Section

Molecular Mechanics Calculations. Computational experiments were performed using an IBM-compatible 486*dx*-50 personal computer running the modified version of MM2(87)[43] for systems containing metal ions described previously.[41] Alchemy III[50] was used to set up molecule data files for MM2 and to plot energy-minimized structures. All geometry optimizations were performed using a cutoff criterion of $\Delta E \leq 0.00012$ kcal·mol^{-1} between successive iterations of MM2's block-diagonalized Newton–Raphson least-squares algorithm.[43] We[41] and others[9] have shown that the principal conformational and structural features of various metalloporphyrins are readily modeled within a "bonded" formalism which ignores the contribution of electrostatic effects to both the coordination geometry of the metal ion and the structure of the porphyrin macrocycle. This approach, used in the present study, has been implemented mainly because there is considerable uncertainty in reliably estimating the charge distribution in the vicinity of the metal ion, and therefore appropriate bond dipole or point charge parameters for the force field.[41] The total strain energy calculated by MM2 from the parameters in the current force field, neglecting charge and dipole terms, is given by eq 1

$$U_T = \sum_{i=1}^{p} U_B + \sum_{j=1}^{q} U_\theta + \sum_{k=1}^{r} U_\phi + \sum_{l=1}^{s} U_{NB} + \sum_{m=1}^{t} U_{SB} \quad (1)$$

where the summations are over all energy contributions from bond stretching (U_B), angle bending (U_θ), torsional angle (U_ϕ), and stretch–bend (U_{SB}) deformations within the molecule, as well as van der Waals interactions (U_{NB}). The nonbonded interaction energy is calculated between all pairs of atoms not bound to each other or to a common atom and is factored into 1,4 (dihedral) and through-space components by MM2. The potential functions constituting the energy terms in eq 1 are those described by Allinger.[43,47c]

Our previous force field[41] for metalloporphyrins contained newly developed parameters for metal ions coordinated by various porphyrin ligands and used the internal parameters of MM2 with SCF π-MO procedures to describe the porphyrin and axial imidazole ligands. Although the inherent parameters in MM2, in conjunction with our newly developed torsional parameters, provided an acceptable model for the conformation of the porphyrin macrocycle as a whole, several calculated bond lengths in the porphyrin poorly matched those observed crystallographically.[51a] We have therefore rederived a force field for all spin and oxidation states of iron porphyrins, mainly from consideration of structural data in the Cambridge Structural Database,[51b] and have dispensed with SCF π-MO calculations altogether, choosing to use a localized bond model instead.[51c] A new force field is, of course, required when changing the MM model from one using a SCF π-MO description of the porphyrin and ligands to one treating all bonds as localized, owing to the poor transferability of force field parameters from one model to another.[47c]

Although MM2 contains parameters for many non-transition elements, it is not designed to perform calculations on complexes of transition metal or lanthanide ions where coordination numbers ≥ 4 are normal, requiring that appropriate parameters be furnished by the user after suitable[41] modification of the program. Figure 11 shows the additional atom types that we have used for parametrization of the force field, while Table 8 lists the new parameters for bond stretching, angle bending, and torsional deformations involving the metal ion, axial ligands, and porphyrin core; the remainder of the force field will be addressed elsewhere.[51c]

The following crystal structures, most of the $[Fe(TMP)]^+$ complexes from low-temperature X-ray diffraction data, were used for parametrization of the force field: *D_{2d}-ruf* $[Fe(TMP)(4\text{-}NMe_2Py)_2]ClO_4$,[21] $[Fe(TMP)(1\text{-}MeIm)_2]ClO_4$,[21] *$D_{2d}$-ruf* $[Fe(TMP)(3\text{-}EtPy)_2]ClO_4$,[42] *$D_{2d}$-ruf* $[Fe(TMP)(4\text{-}CNPy)_2]ClO_4$,[42] *$D_{2d}$-ruf* $[Fe(TMP)(3\text{-}ClPy)_2]ClO_4$,[42] *$D_{2d}$-ruf* $[Fe(TMP)(1,2\text{-}Me_2Im)_2]ClO_4$, *$D_{2d}$-ruf* $[Fe(TPP)(2\text{-}MeHIm)_2]ClO_4$,[52a]

(44) Scheidt, W. R.; Osvath, S. R.; Lee, Y. J. *J. Am. Chem. Soc.* **1987**, *109*, 1958.

(45) Scheidt, W. R.; Geiger, D. K.; Haller, K. J. *J. Am. Chem. Soc.* **1982**, *104*, 495.

(46) (a) Brubaker, G. R.; Johnson, D. W. *Coord. Chem. Rev.* **1984**, *53*, 1. (b) Hancock, R. D. *Prog. Inorg. Chem.* **1989**, *37*, 89. (c) Schwarz, C. L.; Endicott, J. F. *Inorg. Chem.* **1989**, *28*, 4011. (d) Rappé, A. K.; Casewit, C. J.; Colwell, K. S.; Goddard, W. A.; Skiff, W. M. *J. Am. Chem. Soc.* **1992**, *114*, 10024. (e) Weisemann, F.; Teipel, S.; Krebs, B.; Höweler, U. *Inorg. Chem.* **1994**, *33*, 1891. (f) Teuting, J. L.; Spence, K. L.; Zimmer, M. *J. Chem. Soc., Dalton Trans.* **1994**, 551. (g). Lin, W.; Welsh, W. J.; Harris, W. R. *Inorg. Chem.* **1994**, *33*, 884.

(47) (a) Sprague, J. T.; Tai, J. C.; Young, Y.; Allinger, N. L. *J. Comput. Chem.* **1987**, *8*, 581. (b) Burkert, U.; Allinger, N. L. *Molecular Mechanics*; ACS Monograph 177; American Chemical Society: Washington, DC, 1982. (c) Bowen, J. P.; Allinger, N. L. In *Reviews in Computational Chemistry*; Lipkowitz, K. B., Boyd, D. B., Eds.; VCH Publishers: New York, 1991; Vol. 2, p 81.

(48) Tai, J. C.; Allinger, N. L. *J. Am. Chem. Soc.* **1988**, *110*, 2050.

(49) Allinger, N. L.; Rahman, M.; Lii, J. H. *J. Am. Chem. Soc.* **1990**, *112*, 8293.

(50) Commercial molecular mechanics and molecular graphics programs used in this study include the following: (a) Alchemy III, 3D Molecular Modeling Software; Tripos Associates Inc.: 1699 S. Hanley Rd., St. Louis, MO. (b) Xanadu, program for manipulation of crystallographic data: Roberts, P.; Sheldrick, G. M. 1976/7. (c) Axum, Technical Graphics and Data Analysis, V. 3.0; TriMetrix Inc.: 444 NE Ravenna Boulevard, Suite 210, Seattle, WA 98115. (d) Schakal 88, Program for the Graphic Representation of Molecular and Crystallographic Models; Keller, E. Kristallographisches Institut der Universitaet: Hebelstr. 25, D-7800, Freiburg, FRG. (e) Sybyl, Molecular Modeling Software, V. 6.0; Tripos Associates Inc.: 1699 S. Hanley Rd., St. Louis, MO.

(51) (a) For example, C_a-C_m bonds were, in some cases, shorter than those of the crystal structure by as much as 0.056 Å. We have traced this to the SCF-modulation of the stretching (and torsional) constants for C–C bonds within the porphyrin macrocycle by MM2 during refinement. (b) The procedure of using the mean observed angles and interatomic distances from the structural data base for setting the "strain-free" or minimum energy coefficients in the force field affords a rudimentary set of parameters for the potential functions of the MM model; these should then be refined or optimized to achieve accurate structural and conformational models of the compounds of interest.[51c] (c) Marques, H. M.; Munro, O. Q.; Grimmer, N. E.; Levendis, D. C.; Marsicano, F.; Pattrick, G.; Markoulides, T. Manuscript in preparation.

(52) (a) Scheidt, W. R.; Kirner, J. L.; Hoard, J. L.; Reed, C. A. *J. Am. Chem. Soc.* **1987**, *109*, 1963. (b) Higgins, T.; Safo, M. K.; Scheidt, W. R. *Inorg. Chim. Acta* **1991**, *178*, 261. (c) Collins, D. M.; Countryman, R.; Hoard, J. *J. Am. Chem. Soc.* **1972**, *94*, 2066. (d) Inniss, D.; Soltis, S. M.; Strouse, C. E. *J. Am. Chem. Soc.* **1988**, *110*, 5644.

D_{2d}-*sad* [Fe(TPP)(1-MeIm)$_2$]ClO$_4$,[52b] D_{2d}-*ruf* [Fe(TPP)(HIm)$_2$]Cl,[52c] [Fe(TPP)(HIm)$_2$]Cl,[44] D_{2d}-*ruf* [Fe(TPP)(Py)$_2$]ClO$_4$,[52d] [Fe(TPP)(*c*-Mu)]SbF$_6$,[20b] and [Fe(TPP)(*t*-Mu)$_2$]SbF$_6$.[20b] The force field was optimized by adjusting appropriate parameters on a trial-and-error basis until the rmsd's between calculated and crystallographically observed bond lengths, bond angles, and dihedral angles were ≲0.015 Å, <2°, and ≲5.5°, respectively. The similitude of the refined MM and X-ray structural data was assessed by statistically comparing the refined bond lengths, bond angles, and dihedral angles from the MM2 output file to those measured by MM2 from an initial energy calculation, with no geometry optimization, on the X-ray structure. An example of the data thus obtained is given in Table 6 for two extreme conformations of [Fe(TMP)L$_2$]$^+$ complexes.

A further test of the accuracy of the force field involved least-squares fitting of the 25 core atoms and axial ligand donor atoms of the calculated structure to those of the appropriate X-ray structure using the "fit" function of Alchemy III; rmsd's ≲ 0.080 Å were deemed acceptable based on similar data recently reported by Smith, Shelnutt, and co-workers.[36] Four selected examples of this type of comparison are shown in Figure 3. In addition, Xanadu was routinely used to calculate the perpendicular displacements of the various core atoms from the least-squares plane described by the central metal ion and 24 non-hydrogen atoms of the porphyrin macrocycle. Torsional constants controlling the extent of core ruffling were adjusted until the calculated parameters (D_N, C_a, C_b, C_m, C_{av}, and D_{av}, in Table 5, and the dihedral angles, e.g. Table 6) were in good agreement with those of the X-ray structures.

We have used conformational mapping techniques[53] to study the global minima of the strain energy surfaces for four- and six-coordinate [Fe(*meso*-tetraarylporphyrin)]$^+$ complexes, the specific goal of these computational experiments being an assessment of the impact of changing the identity of both the peripheral *meso* substituents and coordinated axial ligands on the global minimum and surrounding region. The experiments were performed by selecting a pair of dihedral angles to opposite *meso*-aryl substituents (see Figure 5a) as the reaction coordinate. Counterrotation of these torsional angles in a four-coordinate complex effects conversion of a planar D_{4h} metalloporphyrin core to one of D_{2d}-*sad*[39] symmetry with adjacent pairs of pyrrole ring β-carbons alternately canted above and below the mean molecular plane. In each grid search experiment, the selected dihedral angles were driven systematically from 40° to 140° in 5° increments, producing 400 conformations which were geometry-optimized by minimizing all other internal degrees of freedom at each increment. Using Wiberg and Boyd's method,[53b] MM2 fixes the driven dihedral angles at the specified values by adding a sizable torsional "driving" potential (eq 2) to the force field.

$$U_{dr} = c_1[1 + \cos i(\chi + c_2)] \qquad (2)$$

The large potential constant c_1 makes the selected torsion angle χ stiffer than the others in the molecule, while the potential minimum is located at the offset value c_2.[53c] Following geometry refinement, the total strain energy of the obtained conformation is recalculated using the normal force field parameters without the strong driving potential, thereby affording the energy of the incremented geometry minus the extra torsional terms. Besides numerous articles describing the successful application of the systematic grid search method,[54] Beech, Cragg, and Drew[55a] have recently shown that this method located the same lowest-energy conformations of the macrocycle [9]aneS$_3$ as conformational searches using either molecular dynamics or a random incremental pulse (rip) algorithm.[55b-d] The strain energy and dihedral angle data at each grid point were extracted from the MM2 output files using a QBasic program prior to importation into Axum for curve-fitting or 3D analysis. Coordinates of selected structures off the strain energy surfaces were obtained from the MM2 output files and plotted using Schakal 88. Finally, molecular (van der Waals) volumes were calculated using Sybyl, Version 6.0, on a Silicon Graphics IRIS Indigo workstation.

Table 1. Crystallographic Data for [Fe(TMP)(1,2-Me$_2$Im)$_2$]ClO$_4$

complex	[Fe(TMP)(1,2-Me$_2$Im)$_2$]ClO$_4$·0.65C$_6$H$_5$Cl·1.05H$_2$O
formula	$FeC_{73.9}H_{73.35}Cl_{1.65}N_8O_{5.05}$
FW, amu	1268.75
a, Å	14.958(24)
b, Å	21.147(21)
c, Å	20.897(32)
β, deg	98.98(12)
V, Å^3	6529(29)
space group	$P2_1/n$
crystal system	monoclinic
Z	4
μ, mm^{-1}	0.362
temp, K	127
R_1	0.072
R_2	0.088

Synthesis and Characterization of [Fe(TMP)(1,2-Me$_2$Im)$_2$]ClO$_4$. All reactions were carried out under argon in Schlenkware. Chloroform, chlorobenzene, and hexane were distilled over calcium hydride. H_2-TMP was synthesized by the procedure of Lindsey.[56] Perchlorato(porphinato)iron(III) derivatives were prepared by modification of reported procedures.[57] *Caution! Perchlorate salts are potentially explosive when heated or shocked.*[58] *Handle them in milligram quantities with care.* [Fe(TMP)(1,2-Me$_2$Im)$_2$]ClO$_4$ was prepared from Fe(TMP)OClO$_3$ (50 mg, 0.053 mmol) dissolved in 10 mL of chlorobenzene in a Schlenk flask and 1,2-dimethylimidazole (100 mg, 1.0 mmol) was added. After the solution was stirred for 2 min, hexane was carefully layered above the chlorobenzene. After 4 days, X-ray quality crystals were harvested. Mössbauer samples were Apiezon N grease suspensions of finely ground single crystals; measurements were performed on a constant acceleration spectrometer. Isomer shifts are quoted relative to iron metal at 300 K.

Structure Determination. A dark purple crystal of [Fe(TMP)(1,2-Me$_2$Im)$_2$]ClO$_4$ with approximate dimensions of 0.33 × 0.33 × 0.13 mm was examined on an Enraf-Nonius FAST area detector diffractometer at 127 K. All measurements were performed with graphite-monochromated Mo Kα radiation. Preliminary examination suggested a four-molecule monoclinic unit cell. A description of the procedures used for cell constant determination and intensity data collection on the area detector instrument has been given elsewhere.[59] Cell constants so determined are given in Table 1. Complete details of the data collection parameters are given in Table S1. Intensity data were corrected for Lorentz and polarization effects. The consequences of absorption were judged small enough to not require correction; this assumption was confirmed by the low merging *R* value. A total of 22 050 observed data ($F_o > 1.9\sigma(F_o)$) were measured and averaged, yielding 8473 unique observed data; the merging $R(F)$ on the observed data was 0.032. These data were used in all subsequent refinements of structure.

The structure was solved by the direct methods program Multan[60] and subsequent difference Fourier syntheses. The crystals were found to contain three solvent molecules in the asymmetric unit: a partially occupied chlorobenzene and two partially occupied water molecules. The chlorobenzene molecule and one water molecule occupy the same region of the asymmetric unit. Occupancy factors for the solvent molecules were established by a combination of initial hand adjustments

(53) (a) Allinger, N. L. *Adv. Phys. Org. Chem.* **1976**, *13*, 1. (b) Wiberg, K. B.; Boyd, R. H. *J. Am. Chem. Soc.* **1972**, *94*, 8426. (c) Burkert, U.; Allinger, N. L. *J. Comput. Chem.* **1982**, *3*, 40.

(54) (a) Dowd, M. K.; Reilly, P. J.; French, A. D. *J. Comput. Chem.* **1992**, *13*, 102. (b) French, A. D. *Biopolymers* **1988**, *27*, 1519. (c) Ha, S. N.; Madsen, L. J.; Brady, J. W. *Biopolymers* **1988**, *27*, 1927. (d) Person, R. V.; Peterson, B. R.; Lightner, D. A. *J. Am. Chem. Soc.* **1994**, *116*, 42. (e) Boiadjiev, S. E.; Person, R. V.; Puzicha, G.; Knobler, C.; Maverick, E.; Trueblood, K. N.; Lightner, D. A. *J. Am. Chem. Soc.* **1992**, *114*, 10123.

(55) (a) Beech, J.; Cragg, P. J.; Drew, M. G. B. *J. Chem. Soc., Dalton Trans.* **1994**, 719. (b) Ferguson, D. M.; Raber, D. J. *J. Am. Chem. Soc.* **1989**, *111*, 4371. (c) Ferguson, D. M.; Glauser, W. A.; Raber, D. J. *J. Comput. Chem.* **1989**, *10*, 903. (d) Ferguson, D. M.; Raber, D. J. *J. Comput. Chem.* **1990**, *11*, 1061.

(56) Lindsey, J. S.; Wagner, W. R. *J. Org. Chem.* **1989**, *54*, 828.

(57) Dolphin, D. H.; Sams, J. R.; Tsin, T. B. *Inorg. Chem.* **1977**, *16*, 711.

(58) Wolsey, W. C. *J. Chem. Educ.* **1973**, *50*, A335. *Chem. Eng. News* **1983**, *61* (Dec. 5), 4; **1963**, *41* (July 8), 47.

(59) Scheidt, W. R.; Turowska-Tyrk, I. *Inorg. Chem.* **1994**, *33*, 1314.

Table 2. Fractional Coordinates for $[Fe(TMP)(1,2\text{-}Me_2Im)_2]ClO_4$[a]

atom	*x*	*y*	*z*	atom	*x*	*y*	*z*
Fe	0.62091(5)	0.23708(3)	0.28851(3)	C(17)	0.8984(4)	0.37520(27)	0.45311(27)
N(1)	0.68775(27)	0.22419(18)	0.37373(18)	C(18)	1.2119(4)	0.2855(4)	0.4672(4)
N(2)	0.70500(27)	0.30370(19)	0.27377(18)	C(19)	0.9554(4)	0.1890(3)	0.3139(3)
N(3)	0.55313(27)	0.24999(18)	0.20207(19)	C(21)	0.6017(4)	0.41153(23)	0.13830(24)
N(4)	0.53777(27)	0.17057(19)	0.30317(19)	C(22)	0.6468(4)	0.42057(26)	0.08507(25)
N(5)	0.6987(3)	0.17790(20)	0.24636(22)	C(23)	0.6341(4)	0.47708(28)	0.05078(27)
N(6)	0.5361(3)	0.29781(22)	0.32171(22)	C(24)	0.5784(4)	0.52367(28)	0.06720(29)
N(7)	0.4647(3)	0.37060(22)	0.36874(22)	C(25)	0.5336(4)	0.51359(26)	0.1193(3)
N(8)	0.7762(3)	0.09979(21)	0.21454(22)	C(26)	0.5445(4)	0.45794(26)	0.15530(27)
C(a1)	0.6556(3)	0.19798(23)	0.42585(23)	C(27)	0.4952(4)	0.44870(28)	0.2128(3)
C(a2)	0.7767(3)	0.24040(24)	0.39470(22)	C(28)	0.5675(5)	0.5848(3)	0.0299(3)
C(a3)	0.7921(3)	0.31057(22)	0.30496(23)	C(29)	0.7067(5)	0.3703(3)	0.06379(29)
C(a4)	0.6890(4)	0.35070(23)	0.22877(23)	C(31)	0.4135(4)	0.10498(24)	0.14587(24)
C(a5)	0.5562(3)	0.30212(23)	0.16390(24)	C(32)	0.4580(4)	0.05288(25)	0.12316(26)
C(a6)	0.4984(3)	0.20620(23)	0.16678(23)	C(33)	0.4087(4)	0.01155(26)	0.07942(27)
C(a7)	0.4810(3)	0.13745(23)	0.25735(24)	C(34)	0.3172(4)	0.02050(28)	0.05727(28)
C(a8)	0.5210(4)	0.15048(24)	0.36275(24)	C(35)	0.2749(4)	0.07120(28)	0.08068(27)
C(b1)	0.7252(4)	0.19961(25)	0.48082(24)	C(36)	0.3210(4)	0.11408(26)	0.12457(26)
C(b2)	0.8007(4)	0.22248(24)	0.46141(24)	C(37)	0.2714(4)	0.1689(3)	0.1492(3)
C(b3)	0.8328(3)	0.36417(25)	0.27828(24)	C(38)	0.2658(5)	−0.0235(3)	0.0080(3)
C(b4)	0.7679(4)	0.39033(25)	0.23307(24)	C(39)	0.5569(4)	0.0414(3)	0.1453(3)
C(b5)	0.5003(4)	0.29166(26)	0.10279(26)	C(41)	0.5454(4)	0.14209(25)	0.48329(25)
C(b6)	0.4676(4)	0.23204(27)	0.10357(23)	C(42)	0.5753(4)	0.08363(27)	0.50837(25)
C(b7)	0.4283(4)	0.09423(26)	0.28902(26)	C(43)	0.5487(4)	0.06395(28)	0.56631(27)
C(b8)	0.4505(4)	0.10373(28)	0.35324(27)	C(44)	0.4939(4)	0.1007(3)	0.59848(27)
C(m1)	0.8300(3)	0.27643(22)	0.35946(22)	C(45)	0.4659(4)	0.1591(3)	0.57267(28)
C(m2)	0.6151(4)	0.35339(24)	0.17845(24)	C(46)	0.4913(4)	0.18057(27)	0.51526(27)
C(m3)	0.4682(3)	0.15013(23)	0.19144(24)	C(47)	0.4603(5)	0.2445(3)	0.4888(3)
C(m4)	0.5735(4)	0.16624(25)	0.42192(24)	C(48)	0.4658(5)	0.0773(4)	0.6604(3)
C(1)	0.7286(4)	0.12053(26)	0.25938(26)	C(49)	0.6363(4)	0.04236(27)	0.47574(28)
C(2)	0.7763(4)	0.14767(29)	0.16850(27)	Cl(1)	1.00359(12)	0.11058(10)	0.10686(9)
C(3)	0.7293(4)	0.19507(26)	0.18783(27)	O(1)	0.9166(4)	0.0921(4)	0.0770(3)
C(4)	0.7146(4)	0.08134(29)	0.31525(27)	O(2)	1.0603(4)	0.1156(4)	0.05888(29)
C(5)	0.8194(5)	0.0397(3)	0.2091(3)	O(3)	0.9981(5)	0.1713(3)	0.1364(3)
C(6)	0.5448(5)	0.34459(29)	0.3627(3)	O(4)	1.0404(7)	0.0687(4)	0.1565(4)
C(7)	0.4379(5)	0.29177(29)	0.2994(3)	O(5)	0.1847(10)	0.0592(7)	0.2666(7)
C(8)	0.3983(4)	0.3366(4)	0.3281(3)	O(6)	0.2383(13)	0.3843(21)	0.1723(17)
C(9)	0.4434(7)	0.4223(4)	0.4083(4)	O(7)	0.1287(15)	0.2878(12)	0.2273(10)
C(10)	0.6292(5)	0.3680(3)	0.3985(3)	Cl(2)	0.28571(25)	0.40335(28)	0.12402(18)
C(11)	0.9288(3)	0.28192(24)	0.38524(24)	C(51)	0.2175(10)	0.3874(8)	0.2056(7)
C(12)	0.9885(4)	0.23802(29)	0.36435(27)	C(52)	0.2310(5)	0.4427(4)	0.2396(4)
C(13)	1.0790(4)	0.2402(3)	0.3919(3)	C(53)	0.1877(6)	0.4367(4)	0.2913(4)
C(14)	1.1121(4)	0.28421(29)	0.4386(3)	C(54)	0.1448(6)	0.3821(5)	0.2967(4)
C(15)	1.0525(4)	0.32761(29)	0.45780(27)	C(55)	0.1526(8)	0.3423(6)	0.2504(5)
C(16)	0.9607(4)	0.32785(26)	0.43134(25)	C(56)	0.1834(12)	0.3410(10)	0.2026(13)

[a] The estimated standard deviations of the least significant digits are given in parentheses.

followed by least-squares refinement of occupancy factors. After least-squares refinement was carried to convergence using anisotropic and isotropic temperature factors (isotropic for all atoms carrying hydrogen atoms), a difference Fourier synthesis suggested probable hydrogen atom positions for most hydrogen atoms in the structure. In particular, at least two probable hydrogen atom positions were found for each methyl group and thus the rotational orientation of all methyl groups was established. Hydrogen atoms were idealized and included in subsequent cycles of least-squares refinement as fixed contributors (C−H = 0.95 Å and $B(H) = 1.2 \times B(C)$) with additional reidealization as required. The structure was then refined to convergence with anisotropic temperature factors for all heavy atoms. There were a total of 811 variables in the final model (data/variable ratio = 10.44); final $R_1 = 0.072$ and $R_2 = 0.088$. Final atomic coordinates are given in Table 2. Anisotropic thermal parameters, fixed hydrogen atom positions, and full tables of bond lengths and bond angles are available as supplementary material. Selected bond lengths and bond angles involving the iron(III) ion and axial ligands are given in Tables 3 and 4, respectively (*vide infra*).

(60) Programs used in this study include local modifications of Main, Hull, Lessinger, Germain, Declerq, and Woolfson's MULTAN, Jacobson's ALLS, Zalkin's FORDAP, Busing and Levy's ORFFE and ORFLS, and Johnson's ORTEP2. Atomic form factors were from: Cromer, D. T.; Mann, J. B. *Acta Crystallogr., Sect. A* **1968**, *A24*, 321. Real and imaginary corrections for anomalous dispersion in the form factor of the iron and chlorine atoms were from: Cromer, D. T.; Liberman, D. J. *J. Chem. Phys.* **1970**, *53*, 1891. Scattering factors for hydrogen were from: Stewart, R. F.; Davidson, E. R.; Simpson, W. T. *J. Chem. Phys.* **1965**, *42*, 3175. All calculations were performed on VAXstation 4000 computers.

Results and Discussion

Molecular Structure of $[Fe(TMP)(1,2\text{-}Me_2Im)_2]ClO_4$. The molecular structure of the $[Fe(TMP)(1,2\text{-}Me_2Im)_2]^+$ cation is shown in Figure 1. As expected from previous work,[19,21,42,52a] the formation of a low-spin iron(III) complex with the sterically bulky 1,2-dimethylimidazole ligands leads to a ruffled porphinato core, the formation of two oblong cavities at right angles on opposite sides of the porphyrin ring, and a relative perpendicular orientation of the two axial imidazole ligands. The projections of the two imidazole planes onto the porphyrin core almost exactly bisect adjacent pairs of N_p-Fe-N_p angles and the dihedral angle between the two imidazole ligands is 89.4°. The two types of $Fe-N_{Im}-C$ angles are distinctly different with the average $Fe-N_{Im}-C(Me)$ angle (134.6°) much larger than the $Fe-N_{Im}-C(H)$ angle (119.8°). This tilting of the imidazole arises from a minimizing of steric interactions of the imidazole α-methyl group with the porphyrin core. The corresponding values of these angles in $[Fe(TPP)(2\text{-}MeHIm)_2]^+$ [52a] are 132.8° and 120.6°; the modestly more equivalent values are

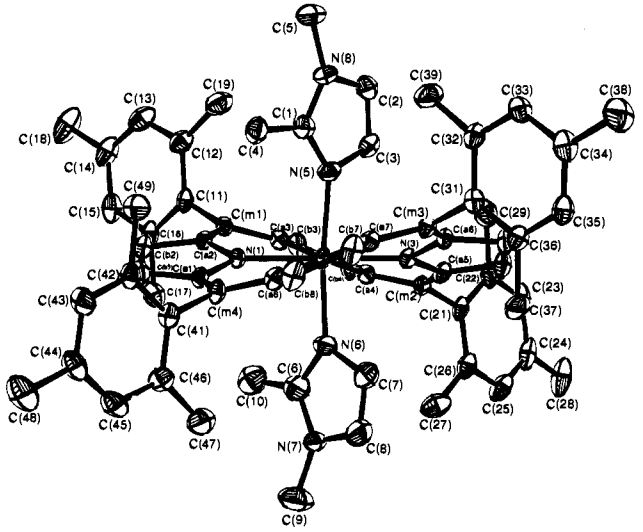

Figure 1. ORTEP diagram of the structure of the $[Fe(TMP)(1,2\text{-}Me_2\text{-}Im)_2]^+$ cation illustrating the atom labeling. Fifty percent probability surfaces are shown. Hydrogen atoms have been omitted for clarity.

the result of the slightly less bulky 2-MeHIm ligand compared to 1,2-Me_2Im. (Tilting values have been tabulated for a series of sterically hindered and unhindered imidazole-ligated complexes in Tables V and VI of ref 61.) All of these stereochemical features are distinctly visible in Figure 1. The dihedral angles of the mesityl groups with the mean plane of the 24-atom porphyrin core are 89.7, 83.3, 87.2, and 87.9°.[62] The role of the hydrogen atoms in these conformational effects can be seen in the ORTEP diagram given in the supplementary material which shows all (idealized) hydrogen atom positions, all of which are derived from experimental evidence (difference Fouriers).

Although the nonplanarity of the porphinato ligand was expected, the exceptionally high degree of nonplanarity, which can be clearly seen in Figure 1, is nonetheless remarkable. Figure 2 shows the perpendicular displacements of each atom, in units of 0.01 Å, from the mean plane of the 25-atom core. The absolute average value of the methine carbon atom displacements, 0.72 Å, is the largest yet observed in an iron(III) porphyrinate complex. Two other, related measures also attest to the extreme nonplanarity of the core. The nonplanarity of the C_m substituents of the pyrrole rings is shown by their average displacement of ±0.22 Å from the mean plane of the individual pyrrole rings (cf. Figure 1). The extreme nonplanarity is also demonstrated by the sum of the angles subtended at the N_p (359.9°), C_a (359.2°), and C_m (359.8°) atoms; all have angle sums less than 360°. This indicates that each atom comprising the inner 16-membered ring of the porphyrin macrocycle is slightly displaced from the local mean plane passing through it and its three attached substituent atoms. This can be seen in Figure 2, where the averaged values of various chemical classes of distances and angles in the core have been entered. By this measure, angular strain is especially prominent at the α carbon atoms (C_a).

Individual values of selected bond distances and angles involving the iron(III) ion are given in Tables 3 and 4 and, as noted, averaged values for the core are entered on Figure 2.[63]

(61) Momenteau, M.; Scheidt, W. R.; Eigenbrot, C. W.; Reed, C. A. *J. Am. Chem. Soc.* **1988**, *110*, 1207.

(62) However, the dihedral angles of any individual mesityl group with its adjacent pair of pyrrole rings are all ~72°.

(63) The number in parentheses following each averaged value is the estimated standard deviation, calculated on the assumption that all averaged values are drawn from the same population.

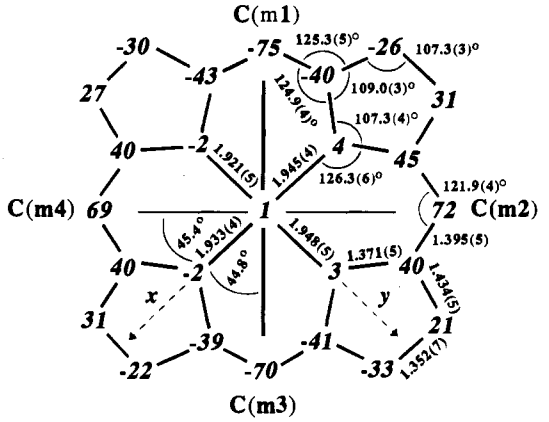

Figure 2. Formal diagram of the porphinato core in $[Fe(TMP)(1,2\text{-}Me_2Im)_2]ClO_4$ displaying the perpendicular displacement, in units of 0.01 Å, of each atom from the mean plane of the 25-atom core. Averaged values for the chemically unique bond distances (in Å) and angles in the porphinato core are shown. The orientations (and angles ϕ) of the axial ligands relative to the Fe−N(4) bond vector are indicated by the heavy line for the above-plane ligand and the thinner line for the below-plane ligand. Individual values of the $Fe-N_p$ bond distances are given, along with the *x*- and *y*-vectors defining the Cartesian axes of the heme group.

Table 3. Selected Bond Distances in $[Fe(TMP)(1,2\text{-}Me_2Im)_2]ClO_4{\cdot}0.65C_6H_5Cl{\cdot}1.05H_2O$[a]

type	length, Å	type	length, Å
Fe−N(1)	1.921(5)	N(6)−C(6)	1.302(8)
Fe−N(2)	1.945(4)	N(6)−C(7)	1.476(9)
Fe−N(3)	1.948(5)	N(7)−C(6)	1.342(8)
Fe−N(4)	1.933(4)	N(7)−C(8)	1.401(8)
Fe−N(5)	2.004 (5)	N(7)−C(9)	1.436 (8)
Fe−N(6)	2.004 (5)	N(8)−C(1)	1.336 (7)
N(5)−C(1)	1.307 (7)	N(8)−C(2)	1.397 (7)
N(5)−C(3)	1.419 (7)	N(8)−C(5)	1.439 (8)

[a] The estimated standard deviations of the least significant digits are given in parentheses.

Table 4. Selected Bond Angles in $[Fe(TMP)(1,2\text{-}Me_2Im)_2]ClO_4{\cdot}0.65C_6H_5Cl{\cdot}1.05H_2O$[a]

type	value, deg	type	value, deg
N(1)FeN(2)	89.64(19)	FeN(4)C(a8)	125.5(3)
N(1)FeN(3)	179.90(17)	FeN(5)C(1)	133.8(4)
N(1)FeN(4)	90.25(19)	FeN(5)C(3)	120.5(4)
N(1)FeN(5)	93.73(20)	FeN(6)C(6)	135.3(5)
N(1)FeN(6)	92.06(21)	FeN(6)C(7)	119.2(4)
N(2)FeN(3)	90.43(18)	C(1)N(5)C(3)	105.7(4)
N(2)FeN(4)	179.74(18)	C(6)N(6)C(7)	105.4(5)
N(2)FeN(5)	87.06(20)	C(6)N(7)C(8)	106.9(5)
N(2)FeN(6)	92.90(21)	C(6)N(7)C(9)	130.3(6)
N(3)FeN(4)	89.68(19)	C(8)N(7)C(9)	122.8(6)
N(3)FeN(5)	86.20(20)	C(1)N(8)C(2)	107.7(5)
N(3)FeN(6)	88.00(20)	C(1)N(8)C(5)	129.8(5)
N(4)FeN(5)	92.71(21)	C(2)N(8)C(5)	122.5(5)
N(4)FeN(6)	87.34(21)	N(5)C(1)N(8)	111.2(5)
N(5)FeN(6)	174.20(19)	N(5)C(1)C(4)	126.9(5)
FeN(1)C(a1)	126.6(3)	N(8)C(1)C(4)	121.9(5)
FeN(1)C(a2)	126.6(3)	C(3)C(2)N(8)	106.3(5)
FeN(2)C(a3)	126.3(3)	C(2)C(3)N(5)	109.1(5)
FeN(2)C(a4)	126.1(3)	N(6)C(6)N(7)	112.0(6)
FeN(3)C(a5)	126.5(3)	N(6)C(6)C(10)	126.0(6)
FeN(3)C(a6)	125.8(3)	N(7)C(6)C(10)	122.0(6)
FeN(4)C(a7)	127.3(3)	C(7)C(8)N(7)	108.7(6)

[a] The estimated standard deviations of the least significant digits are given in parentheses.

There are several noteworthy features of the averaged bond parameters of $[Fe(TMP)(1,2\text{-}Me_2Im)_2]^+$ that apparently reflect the core accommodations required to allow iron(III) to bind 1,2-

dimethylimidazole. As noted above, the porphinato core has become strongly ruffled in order to minimize the nonbonded contacts between the imidazole methyl and core atoms. This strong ruffling leads to the extremely short mean Fe−N_p distance of 1.937(12) Å, with the shortest observed distance (Table 3) at 1.921(5) Å and the longest at 1.948(5) Å. In contrast, the MM calculations (*vide infra*) predict nearly equivalent Fe−N_p bonds for [Fe(TMP)(1,2-Me_2Im)$_2$]$^+$ with a mean distance of 1.946(1) Å. Asymmetry in the coordination sphere of the metal ion would, with the current MM model, only be predicted if steric in origin. Thus, the observed asymmetry in the equatorial Fe−N_p bonds of the X-ray structure may reflect some measure of experimental uncertainty, but more interestingly, it could indicate an unusual electronic effect operating in the equatorial plane of the complex. Using EPR spectroscopy in conjunction with X-ray crystallography, we[42] have shown that the unpaired electron in [Fe(TMP)(4-NMe_2Py)$_2$]$^+$, with strongly basic axial ligands, resides mainly in the d_{xz} orbital, while the ground state for [Fe(TMP)(4-CNPy)$_2$]$^+$, with weakly basic axial ligands, is inverted with the unpaired spin localized in the d_{xy} orbital. The mean Fe−N_p distance is 1.964(10) Å in the former complex and 1.961(7) Å in the latter. Since the Fe−N_p bonds are, within experimental error, equivalent, the difference in the electronic configuration at the metal is mainly controlled by the electronic character of the axial ligands, presumably with the electron-deficient 4-CNPy ligand stabilizing the filled d_{xz} and d_{yz} orbitals by M → L π-bonding. Localization of the unpaired spin (or hole) in the d_{xy} orbital in [Fe(TMP)(4-CNPy)$_2$]$^+$ may, however, also require increased σ-donation from the porphinato ligand in the *xy* plane, i.e., ruffling of the core and partial contraction of the Fe−N_p bonds. The extreme ligand-induced D_{2d} ruffling in [Fe(TMP)(1,2-Me_2Im)$_2$]$^+$, with concomitant contraction of the *xy* M−L bonds, may favor a shift in the spin distribution within the d-orbital manifold to the extent that a significant proportion of unpaired spin resides in d_{xy}. Electronic and steric effects could, under such circumstances, operate collectively to determine bonding between the iron(III) ion and the porphyrin macrocyle; considerable asymmetry in the Fe−N_p bonds may then result as competition between equatorial electronic and axial steric effects comes into play.

To our knowledge, the Fe−N_p distance of 1.937(12) Å is the shortest such distance reported for an iron porphyrinate, though the degree of ruffling is such that even shorter Fe−N_p distances would be expected.[64a] A D_{2d}-*ruf* distortion of the porphyrin core results in marked contraction along the Fe−N_p bond vectors due to out-of-plane tilting of the pyrrole rings and their rotation about the Fe−N_p bonds.[64b] With sterically hindered axial ligands, however, there must be a limit to the extent to which the core can contract, based on the juxtaposition of the axial ligands and the C_m carbon atoms (cf. Figure 2) and the fact that even though ruffling of the core alleviates ligand-to-porphyrin steric interactions steric strain is still likely to build up between the ligands and the C_a and C_m atoms of the core. This, evidently, leads to the remaining unusual parameters for the apparent core size: relative to other iron(III) porphyrins,[66] short N_p−C_a and long C_a−C_m bond lengths, in conjunction with large C_a−N_p−C_a and small N_p−C_a−C_b and N_p−C_a−C_m bond angles.

Mössbauer Spectra of [Fe(TMP)(1,2-Me_2Im)$_2$]$^+$. The Mössbauer parameters have been measured at intermediate temperatures in zero magnetic field. (The spectrum is very broad at 4.2 K, reflecting intermediate spin relaxation effects.) The compound displays a quadrupole doublet with $\Delta E_Q = 1.25$ mm/s and an isomer shift of 0.14 mm/s at 250 K. At 120 K, the values are 1.26 and 0.17 mm/s. The low value of the quadrupole splitting constant is consistent with previous observations[21,42,67] that ΔE_Q values $\leq$2.0 mm/s suggest relative perpendicular orientations of the axial ligands. The 1.25 mm/s value observed in the present case is lower than the 1.48 mm/s value observed for [Fe(TMP)(2-MeHIm)$_2$]$^+$ [42] or the 1.77 mm/s value observed for [Fe(TPP)(2-MeHIm)$_2$]$^+$.[21] However, ΔE_Q values as small or smaller have been observed in some pyridine derivatives known to have perpendicular axial ligand orientations: 1.25 mm/s for [Fe(TPP)(Py)$_2$]$^+$ [52d,68] and [Fe(TMP)(3-EtPy)$_2$]$^+$ [42] and 0.97 mm/s for [Fe(TMP)(4-CNPy)$_2$]$^+$.[42]

Molecular Mechanics. Fe−N_p and Fe−N_{ax} Compression Parameters. The derivation of parameters for a force field being used to model any class of complexes requires that certain structural or conformational features are identified as being characteristic of that class of compounds and therefore essential to reproduce accurately. One such feature for low-spin ferric porphyrins is the Fe−N_p bond length; this exhibits a marked contraction when the core conformation changes from planar (D_{4h}) to ruffled (D_{2d}). Thus, while the mean Fe−N_p bond length in planar [Fe(TPP)(HIm)$_2$]$^+$ [44] is 1.993(3) Å (axial imidazole planes eclipsed), it is considerably shorter in S_4-ruffled [Fe(TPP)(2-MeHIm)$_2$]$^+$,[52a] measuring 1.971(4) Å, and is shorter still in the present structure of [Fe(TMP)(1,2-Me_2Im)$_2$]$^+$ at 1.937(12) Å. It is noteworthy that the axial ligand planes in the latter S_4-ruffled complexes exhibit relative perpendicular orientations, and therefore that the change in porphyrin core conformation from planar (relatively long Fe−N_p bond lengths) to ruffled (relatively short Fe−N_p bond lengths) is driven principally by changes in the symmetry of the nonbonded interactions between the porphyrin core and the axial ligands. It is unlikely that electronic effects alone, in the absence of ligand-induced ruffling of the porphyrin core, could lead to changes in the Fe−N_p bonds of this magnitude (>0.020 Å). The present force field was therefore optimized to model as accurately as possible this degree of structural flexibility in the equatorial M−L bonds using a single compression parameter for the Fe−N_p bonded interaction (Table 8). We have found that it is important to have a good model of the porphyrin macrocycle[51c] prior to the development of parameters for the metal−ligand interactions since parameters in the force field are inevitably correlated.[53c]

The Fe−N_{ax} bond lengths to sterically restricted imidazoles such as 2-MeHIm and 1,2-Me_2Im average 2.013(6) Å in [Fe(TPP)(2-MeHIm)$_2$]$^+$ [52a] and 2.004(5) Å in [Fe(TMP)(1,2-Me_2-

(64) (a) Hoard, J. L. *Ann. N.Y. Acad. Sci.* **1973**, *206*, 18. (b) It is interesting to note that although the D_{2d}-*sad* [M(OETPP)]$^{n+}$ complexes reported by Sparks *et. al.*,[36] where M = Cu(II) (X-ray structure) and Fe(III) (MM structure), are more highly distorted than D_{2d}-*ruf* [Fe(TMP)(1,2-Me_2Im)$_2$]$^+$, they exhibit *longer* M−N_p bond distances. This reflects the fact that a D_{2d}-*sad* core conformation, as found in the [M(OETPP)]$^{n+}$ complexes, is a less efficient stereochemical pathway for contraction of the macrocycle cavity than a D_{2d}-*ruf* core conformation. In illustration, the structure of the D_{2d}-*ruf* [Cu(TPP)] complex reported by Fleischer *et al.*[65] exhibits a *moderately ruffled* core (D_{av} = 0.18 Å) with a mean Cu−N_p distance of 1.981(7) Å, which is actually equivalent to that found in the D_{2d}-*sad* [Cu(OETPP)][36] complex (1.977(5) Å) where the core is *highly ruffled* (D_{av} = 0.70 Å). The exact symmetry of the core distortion therefore appears to be a critical determinant of cavity diameter.

(65) Fleischer, E. B.; Miller, C. K.; Webb, L. E. *J. Am. Chem. Soc.* **1964**, *86*, 2342.

(66) The mean bond lengths and angles presented in Figure 2 for [Fe(TMP)(1,2-Me_2Im)$_2$]$^+$ were compared to the following mean values (672 observations) for iron(III) porphyrins obtained from a search of the Cambridge Data Base: N_p−C_a = 1.381(14) Å, C_a−C_m = 1.388(16) Å, C_a−C_b = 1.437(17) Å, C_b−C_b = 1.350(21) Å, C_a−N_p−C_a = 105.8(1.1)°, N_p−C_a−C_b = 109.8(1.2)°, N_p−C_a−C_m = 125.3(1.4)°.

(67) Medhi, O. K.; Silver, J. *J. Chem. Soc., Dalton Trans.* **1990**, 263, 555.

(68) Epstein, L. M.; Straub, D. K.; Maricondi, C. *Inorg. Chem.* **1967**, *6*, 1720.

Table 5. Comparison of Selected Calculated (Molecular Mechanics) and Observed (X-ray) Structural Data for Low-Spin Complexes of $[Fe(TMP)]^+$ [a]

(A) Bispyridine Complexes

	3-ClPy		3-EtPy		4-CNPy	
	obs[b]	calc	obs[b]	calc	obs[b]	calc
$Fe-N_p$[c]	1.968(3)	1.966(4)	1.964(4)	1.963(0)	1.961(7)	1.961(0)
$Fe-N_{ax}$[c]	2.012(8)	2.008(3)	1.996(9)	2.001(0)	2.011(14)	2.004(0)
C_a[d]	21(4)	24(4)	25(3)	26(1)	25(3)	27(0)
C_b[d]	14(8)	16(9)	17(6)	18(1)	17(6)	18(0)
C_m[d]	36(4)	46(0)	43(2)	51(1)	41(3)	53(0)
C_{av}[d]	21(0)	25(13)	26(10)	28(12)	25(10)	29(13)
D_N[d]	4(3)	2(1)	3(3)	1(1)	4(1)	0(0)
D_{av}[d]	18(11)	21(15)	21(13)	22(15)	20(13)	23(16)
ϕ_1[e]	42.0	42.0[f]	43.0	44.8	43.0	45.0
ϕ_2[e]	29.0	29.0[f]	43.0	44.2	44.0	45.0
$\Delta\phi_e$	71.0	71.0[f]	86.0	89.0	87.0	90.0

(B) Bisimidazole Complexes

	1,2-Me_2Im		1-MeIm[i]		1-MeIm[j]	
	obs[g]	calc	obs[h]	calc	obs[h]	calc
$Fe-N_p$[c]	1.937(12)	1.946(1)	1.988(14)	1.983(5)	1.987(1)	1.985(1)
$Fe-N_{ax}$[c]	2.004(5)	2.007(1)	1.974(0)	1.973(1)	1.964(0)	1.964(0)
C_a[d]	41(2)	35(1)	1(1)	1(1)	4(3)	1(0)
C_b[d]	28(4)	23(2)	2(1)	3(1)	7(2)	1(1)
C_m[d]	72(3)	68(1)	1(1)	1(1)	8(1)	1(1)
C_{av}[d]	42(17)	37(16)	1(1)	2(1)	6(3)	1(1)
D_N[d]	3(1)	2(2)	2(1)	2(1)	3(1)	3(0)
D_{av}[d]	34(22)	30(20)	1(1)	2(1)	5(3)	1(1)
ϕ_1[e]	45.5	44.0	26.4	26.4[f]	43.1	43.1[f]

[a] $Fe-N_p$ is the mean metal−porphyrin nitrogen bond length; $Fe-N_{ax}$ is the mean metal−axial donor atom distance; C_a, C_b, C_m, and C_{av} are the mean absolute perpendicular displacements of the α, β, *meso*, and all carbon atoms from the mean plane through the 25-atom core of the iron(III) porphyrin, respectively; D_N and D_{av} are the mean absolute perpendicular displacements of the porphinato nitrogens and all the core atoms from the mean plane through the 25-atom core, respectively. The number in parentheses following each averaged absolute value is the estimated standard deviation (esd), calculated on the assumption that all averaged values are drawn from the same population. Where the esd is zero, all atoms of that type are equally displaced from the mean plane. ϕ_i refers to the orientation of an axial ligand plane projected onto the porphyrin core, relative to an in-plane $Fe-N_p$ vector, and $\Delta\phi$ refers to the relative orientations of the two axial ligand planes. [b] Reference 42. [c] Bond lengths in Å. [d] Displacements in units of 0.01 Å. [e] Orientations in deg; there are no esd's for these data since only one dihedral angle is needed to define the orientation of each ligand. [f] Axial ligand planes locked at X-ray values during structural refinement. [g] This work. [h] Reference 21. [i] Molecule 1 in the unit cell. [j] Molecule 2 in the unit cell.

$Im)_2]^+$. Although these observed axial M−L distances are equivalent (within the esd's of each crystallographic experiment), our MM calculations using an $Fe-N_{ax}$ compression parameter with $k_s = 1.580$ mdyn-Å^{-1} and $\ell_0 = 1.950$ Å (Table 8) do model the apparent variation by predicting values of 2.014 Å for $[Fe(TPP)(2\text{-MeHIm})_2]^+$ and 2.007 Å for $[Fe(TMP)(1,2\text{-}Me_2Im)_2]^+$ (Table 5). As noted above, 1,2-Me_2Im is sterically more hindered than 2-MeHIm so that the relative order of the above $Fe-N_{ax}$ bond lengths appears to be contrary to expectation, especially since the mean calculated $Fe-N_{ax}$ distance (2.014(0) Å) for $[Fe(TPP)(2\text{-MeHIm})_2]^+$ is marginally shorter than that calculated for $[Fe(TPP)(1,2\text{-}Me_2Im)_2]^+$ (2.016(0) Å, data not shown). Overall, these results suggest that there is an axial ligand−*meso*-mesityl nonbonded interaction in $[Fe(TMP)(1,2\text{-}Me_2Im)_2]^+$ which is capable of *enhancing* ruffling of the porphyrin core, leading to the development of deeper pockets beneath the planes of the axial ligands, which then approach the porphyrin core more closely. The absence of such an effect in $[Fe(TPP)(2\text{-MeHIm})_2]^+$ means that although the 2-MeHIm ligands are sterically less hindered than the 1,2-Me_2Im ligands, they cannot approach the (less ruffled) porphyrin core as closely as the ligands in $[Fe(TMP)(1,2\text{-}Me_2Im)_2]^+$; the calculated and observed $Fe-N_{ax}$ distances are therefore slightly longer to 2-MeHIm in the iron(III) TPP complex.

Calculated Low-Spin Iron(III) Complexes of TMP. Figure 3 compares selected calculated D_{2d}-*ruf* and planar low-spin ferric TMP complexes with the corresponding X-ray structures. Superposition of the structures was achieved by fitting (least-squares) the 25 core atoms and two axial ligand donor atoms of the calculated structures to those of the X-ray structures. The root-mean-square differences were 0.061 ($[Fe(TMP)(1,2\text{-}Me_2Im)_2]^+$), 0.080 ($[Fe(TMP)(4\text{-}NMe_2Py)_2]^+$), 0.062 ($[Fe(TMP)(3\text{-ClPy})_2]^+$), and 0.057 Å ($[Fe(TMP)(1\text{-MeIm})_2]^+$); these compare favorably with similar data reported by Sparks *et al.*,[36] thereby confirming the accuracy of the force field. The calculated structures are seen to deviate somewhat from the X-ray structures in the region of the peripheral mesityl substituents. This is mainly due to the fact that, for the X-ray structures, intermolecular nonbonded contacts within the crystal lattice are capable of promoting tilting of the peripheral groups,[40,41] particularly *meso*-aryl substituents, which then take on a range of orientations relative to the mean plane of the porphyrin. The sterically favored orientation is typically ~90° (colinear with the heme normal) in complexes without *sad*-distorted cores. Minor deviations from this, however, have no serious effect on the porphyrin core conformation, and we have previously shown[41] that in *four-coordinate* complexes, aryl dihedral angles (χ) much lower than 90° are required before significant distortion of the metalloporphyrin core results. (In *six-coordinate* complexes, where the core conformation is controlled largely by the nature and orientations of the axial ligands, even large rotations of the *meso*-mesityl groups have a negligible effect on the geometry of the metalloporphyrin core (*vide infra*).)

Axial ligands such as 4-NMe_2Py are more powerful σ-donors than normal alkylpyridines or halopyridines[45,69] and should

(69) Ramsey, B. G.; Walker, F. A. *J. Am. Chem. Soc.* **1974**, *96*, 3314.

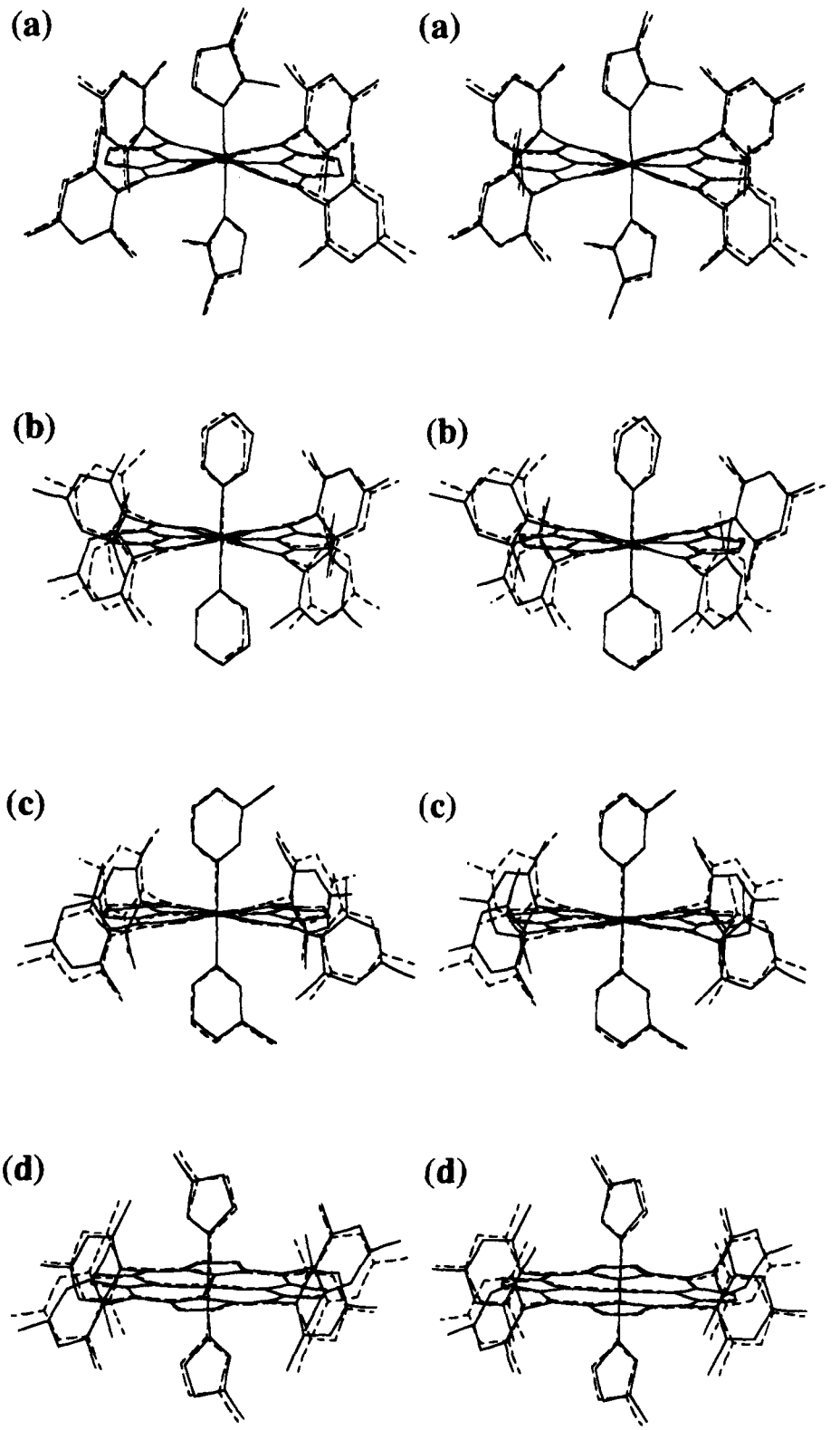

Figure 3. Stereoview comparing superimposed calculated (dashed lines) and observed (solid lines) six-coordinate low-spin complexes of $[Fe(TMP)]^+$. The X-ray structures to which the calculated structures have been fitted are (a) $[Fe(TMP)(1,2\text{-}Me_2Im)_2]^+$ and (b) $[Fe(TMP)(4\text{-}NMe_2Py)_2]^+$ [21] (both without the 4-NMe_2 group for clarity), (c) $[Fe(TMP)(3\text{-}ClPy)_2]^+$,[42] and (d) $[Fe(TMP)(1\text{-}MeIm)_2]^+$.[21] Hydrogen atoms have been omitted for clarity. The 25 core atoms and two axial ligand donor atoms were superimposed by least-squares optimization; the rmsd's are (a) 0.061 Å, (b) 0.080 Å, (c) 0.062 Å, and (d) 0.057 Å. The mean absolute differences (and esd's) between *all* calculated and observed bond lengths, bond angles, and torsional angles are the following: (a) 0.010 (9) Å, 0.36 (35)°, and 1.9 (2.3)°, respectively; (b) 0.004 (3) Å, 0.28 (34)°, and 1.8 (1.8)°, respectively; (c) 0.009 (9) Å, 0.49 (45)°, and 1.7 (1.8)°, respectively; and (d) 0.007 (8) Å, 0.34 (45)°, and 1.6 (1.7)°, respectively.

therefore form stronger (shorter) bonds to the metal ion in a metalloporphyrin. Figure 3 shows that by using a unique Fe–N_{ax} compression parameter (Table 8) for the 4-N-substituted class of pyridines to simulate a stronger metal–ligand bonded interaction, the shorter Fe–N_{ax} bonds to the 4-NMe_2Py ligands in $[Fe(TMP)(4\text{-}NMe_2Py)_2]^+$, and hence the strongly ruffled porphyrin core, are correctly predicted. The data contained in Table 5 indicate that the calculated structural parameters for a

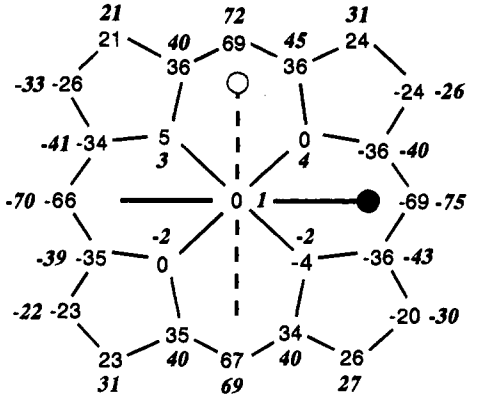

Figure 4. Formal diagram of the porphinato core in the observed (X-ray) and calculated (energy-minimized) structure of $[Fe(TMP)(1,2\text{-}Me_2Im)_2]^+$. Deviations of each non-hydrogen atom from the mean plane of the core (in units of 0.01 Å) are shown. Data for the calculated structure are centered at the usual atomic positions of the metalloporphyrin core, while the crystallographic data for the observed structure are listed in bold italics adjacent to the appropriate atom locations. Also shown are the planes of each axial ligand; the upper ligand is given as the solid line in this perspective. The mean absolute deviations for the various atom types, and the exact axial ligand orientations are listed in Table 5.

range of low-spin iron(III) complexes of TMP are overall in consonance with those determined by X-ray crystallography.

Table 6 compares selected observed (X-ray) and calculated (energy-minimized) bond lengths, bond angles, and torsional angles for $[Fe(TMP)(1\text{-}MeIm)_2]^+$[21] and $[Fe(TMP)(1,2\text{-}Me_2Im)_2]^+$. From Table 6, the mean absolute differences (and esd's) between the observed and calculated bond lengths, bond angles, and torsional angles in $[Fe(TMP)(1,2\text{-}Me_2Im)_2]^+$ are 0.010(9) Å, 0.36 ± 0.35°, and 1.9 ± 2.3°, respectively, while analogous parameters for $[Fe(TMP)(1\text{-}MeIm)_2]^+$ are 0.007 (8) Å, 0.34 ± 0.45°, and 1.6 ± 1.7°. (Similar data were obtained for all complexes used for parametrization of the force field, with individual differences between calculated and observed torsional angles $\lesssim$5.5° in all cases. Further statistics are given in the caption to Figure 3.) The very good agreement between the calculated and observed structures suggests that the present valence bond force field is sufficiently refined to deal with low-spin iron(III) TMP complexes ranging from those with planar cores ($[Fe(TMP)(1\text{-}MeIm)_2]^+$)[21] to those exhibiting strong D_{2d} ruffling ($[Fe(TMP)(1,2\text{-}Me_2Im)_2]^+$).[70] Moreover, the data in Table 6 reveal that even though a bulky ligand like 1,2-Me_2Im is capable of enhancing distortion of the TMP macrocycle, which allows stronger Fe−N_{ax} bonding, the steric bulk of the ligand in the region of the α-methyl group actually limits the approach distance (axial bond length) to Fe−N_{ax} > 2.00 Å. 1-MeIm, on the other hand, is sterically less hindered than 1,2-Me_2Im and therefore achieves shorter Fe−N_{ax} distances ($\gtrsim$ 1.96 Å), while an N-donor ligand like N_3^-, which is minimally hindered, realizes the shortest axial bond lengths (Fe−N_{ax} $\gtrsim$ 1.93 Å[71b]).

Sterically hindered axial ligands such as 2-MeHIm, 1,2-Me_2-Im, and BzHIm in low-spin complexes of iron(III) porphyrins are normally oriented so that $\phi_1 \approx \phi_2 \approx 45°$, with $\Delta\phi \approx 90°$. (The ligand orientation angle ϕ was first used by Hoard[52c] to describe the angle between the line of projection of an axial ligand plane onto the metalloporphyrin core and an in-plane M−N_p bond vector. The relative orientations of the axial ligand planes are then described by $\Delta\phi$.) Depending on the distribution of steric bulk in the axial ligands, one might expect that the observed distortion of the porphyrin core would reflect a response to the specific nature of the geometry of the axial ligand−porphyrin interaction. The map comparing the calculated and observed core conformations of $[Fe(TMP)(1,2\text{-}Me_2Im)_2]^+$ shown in Figure 4 clearly indicates that the asymmetric distribution of steric bulk associated with the α-methyl groups of the axial ligands enhances the distortion of the porphyrin macrocycle directly beneath the ligand methyl groups. The porphyrin conformation is therefore critically dependent on the nature of the axial ligands and their orientations above the plane of the macrocycle.

***D_{2d}-sad* Core Deformations in (*meso*-Tetraarylporphinato)iron(III) Complexes.** We have used the systematic grid search facility of MM2 to investigate the strain energy surfaces of three hypothetical *four-coordinate* low-spin iron(III) complexes, $[Fe(TPP)]^+$, $[Fe(T\text{-}2,6\text{-}Cl_2PP)]^+$, and $[Fe(TMP)]^+$, principally in the global minimum region of conformational space in each case.[73] The main objective of these calculations is to show that in *four-coordinate* complexes, severe D_{2d}-*sad* distortions of the metalloporphyrin core may arise from changes in the orientations of the *meso*-aryl groups, and that the magnitude of the *sad* distortion (it is not a true, stable conformation of the porphyrin macrocycle in simple tetraarylporphyrin species) depends on the steric bulk of the *meso* substituents.

(70) Some of the structural refinements (Tables 5 and 6) have been effected by restriction of the axial ligand planes to the values of ϕ[71a] observed in the X-ray structures of the complexes. The reason for this is that the exact conformation of the porphyrin core in these bisimidazole and bispyridine complexes is strongly dependent on the orientations of the axial ligands. Thus, for example, the core conformation when the axial ligands are oriented so that $\phi_1 = \phi_2 = 45°$, with $\Delta\phi = 90°$, is substantially more ruffled than when $\phi_1 = \phi_2 = 10°$ and $\Delta\phi = 20°$. An accurate assessment of how well the force field models a particular X-ray structure, especially the conformation of the porphyrin core, therefore requires that the axial ligands be set at the observed (X-ray) orientations during refinement. This requirement stems from the fact that the sterically favored orientation occurs at $\phi = 45°$, which represents a minimum in the nonbonded interactions between the axial ligand and the porphyrin core, and that in the absence of a partly constrained refinement all planar axial ligands assume an orientation close to this minimum. The observation that many low-spin pyridine and imidazole complexes of iron(III) porphyrins exhibit ligand plane orientations closer to $\phi = 0°$ than $\phi = 45°$ has been attributed to axial L → M π-bonding,[32] which, in the present context, would require a model incorporating both semiempirical MO and molecular mechanics computational methods.

(71) (a) The nomenclature concerning the orientation of planar axial ligands in metalloporphyrins was first dealt with by Hoard and coworkers: ref 52c. (b) Zhang, Y.; Hallows, W. A.; Ryan, W. J.; Jones, J. G.; Carpenter, G. B.; Sweigart, D. A. *Inorg. Chem.* **1994**, *33*, 3306.

(72) The calculated core geometry is overall somewhat less ruffled than that of the X-ray structure (Table 5), and this is seen to arise mainly from the lower degree of ruffling calculated in the region furthest away from the methyl groups of the axial ligands. Intermolecular lattice interactions[40] and experimental error are likely contributors to the additional distortion of the porphyrin core in the X-ray structure (over and above that enforced by the axial ligands). The MM-calculated core geometry, normally more symmetrical than an experimental geometry, will itself also not be perfect. These three factors will collectively lead to differences between observed and calculated structures in all cases, including that of $[Fe(TMP)(1,2\text{-}Me_2Im)_2]^+$ in Figure 4.

Table 6. Comparison of Calculated (Molecular Mechanics) and Observed (X-ray) Bond Lengths, Bond Angles, and Torsional Angles for Representative Planar and Ruffled Low-Spin Iron(III) TMP Complexes[a]

(A) Bond Lengths (Å)

	$[Fe(TMP)(1,2\text{-}Me_2Im)_2]^+$			$[Fe(TMP)(1\text{-}MeIm)_2]^+$		
bonds	obs[b]	calc	diff	obs[c]	calc	diff
$Fe-N_p$	1.937(12)	1.946(2)	−0.009	1.987(1)	1.985(1)	0.002
$Fe-N_{ax}$	2.004(0)	2.007(1)	0.003	1.965(0)	1.964(0)	0.000
N_a-C_a	1.372(4)	1.384(0)	−0.011	1.382(3)	1.385(1)	−0.003
N_b-C_a	1.370(4)	1.384(0)	−0.014	1.377(3)	1.385(1)	−0.008
C_L-N_L	1.385(57)	1.377(56)	0.009	1.344(60)	1.374(56)	−0.030
C_a-C_b	1.435(4)	1.437(0)	−0.002	1.427(3)	1.438(1)	−0.011
C_a-C_m	1.395(5)	1.392(1)	0.003	1.385(6)	1.390(0)	−0.005
C_b-C_b	1.352(6)	1.345(1)	0.007	1.342(4)	1.343(0)	−0.001
C_m-C_p	1.495(6)	1.503(1)	−0.008	1.503(1)	1.504(1)	−0.001
C_p-C_p	1.390(9)	1.398(1)	−0.009	1.386(9)	1.398(2)	−0.012
C_L-C_L	1.389(73)	1.427(79)	−0.037	1.334(0)	1.350(0)	−0.017

(B) Bond Angles (deg)

	$[Fe(TMP)(1,2\text{-}Me_2Im)_2]^+$			$[Fe(TMP)(1\text{-}MeIm)_2]^+$		
angles	obs[b]	calc	diff	obs[c]	calc	diff
N_a-Fe-N_a	179.9(0)	180.0(0)	−0.06	180.0(0)	179.9(0)	0.13
N_b-Fe-N_b	179.7(0)	179.3(0)	0.44	180.0(0)	179.9(0)	0.12
N_a-Fe-N_{ax}	90.0(3.0)	90.0(2.3)	0.00	90.0(8)	90.0(5)	0.00
N_b-Fe-N_{ax}	90.0(2.8)	90.0(2.2)	−0.01	90.0(3)	90.0(5)	0.00
$N_{ax}-Fe-N_{ax}$	174.2(0)	175.4(0)	−1.23	180.0(0)	179.7(0)	0.25
N_a-Fe-N_b	90.0(4)	90.0(4)	0.00	90.0(1.4)	90.0(7)	0.00
$Fe-N_a-C_a$	126.4(4)	126.7(1)	−0.29	127.1(1.3)	127.3(5)	−0.22
$Fe-N_b-C_a$	126.3(6)	126.6(1)	−0.31	127.3(1.0)	127.3(5)	−0.03
$C_a-N_a-C_a$	107.2(4)	106.7(1)	0.50	105.8(0)	105.3(0)	0.43
$C_a-N_b-C_a$	107.4(2)	106.6(0)	0.71	105.4(0)	105.3(0)	0.07
$N_a-C_a-C_b$	108.9(3)	108.9(1)	0.01	109.6(1)	110.0(1)	−0.32
$N_b-C_a-C_b$	109.0(2)	109.0(0)	0.09	109.9(2)	110.0(1)	−0.05
$N_a-C_a-C_m$	124.8(4)	124.7(1)	0.11	126.1(1)	126.4(4)	−0.28
$N_b-C_a-C_m$	124.9(3)	124.7(0)	0.15	125.9(2)	126.5(4)	−0.52
$C_m-C_a-C_b$	125.5(5)	126.2(1)	−0.73	124.2(1)	123.6(3)	0.56
$C_a-C_b-C_b$	107.3(3)	107.7(0)	−0.37	107.4(2)	107.4(0)	0.04
$C_a-C_m-C_a$	121.9(3)	121.8(1)	0.16	123.3(9)	122.5(9)	0.75
$C_a-C_m-C_p$	119.0(8)	118.9(2)	0.06	118.4(1.2)	118.7(5)	−0.34
$C_m-C_p-C_p$	119.8(1.5)	119.4(1.3)	0.44	119.9(1.0)	119.5(3)	0.41
$C_p-C_p-C_p$	120.0(1.5)	120.0(1.5)	0.00	120.0(1.7)	120.0(1.4)	−0.01
$N_L-C_L-C_L$	116(8.4)	116(8.1)	−0.82	108.7(2.1)	109.1(1.6)	−0.33
$Fe-N_{ax}-C_L$	127(7.4)	128(5.6)	−0.76	128.9 (6)	128.2(4)	0.67
$C_L-N_L-C_L$	116(10.3)	116(10.4)	0.36	116(11.5)	116(11.0)	−0.34
$N_L-C_L-N_L$	111.6(4)	110.6(0)	0.93	114.0(0)	111.9(0)	2.15

(C) Torsional Angles (deg)

	$[Fe(TMP)(1,2\text{-}Me_2Im)_2]^+$			$[Fe(TMP)(1\text{-}MeIm)_2]^+$		
torsions	obs[b]	calc	diff	obs[c]	calc	diff
$C_a-N_a-Fe-N_b$	21.8(2.5)	18.4(1.1)	3.40	1.8(1.0)	0.8(0.6)	1.00
$C_a-N_b-Fe-N_a$	21.9(2.0)	18.3(2.7)	3.60	2.6(1.2)	1.0(0.9)	1.60
$Fe-N_a-C_a-C_b$	177.2(1.8)	179.0(0.1)	−1.81	174.7(0.1)	179.4(0.5)	−4.64
$Fe-N_b-C_a-C_b$	177.7(1.5)	175.9(1.0)	1.78	178.5(0.6)	178.7(0.4)	−0.11
$Fe-N_a-C_a-C_m$	10.0(2.9)	4.7(0.1)	5.27	6.3(0.1)	0.6(0.1)	5.72
$Fe-N_b-C_a-C_m$	10.0(2.7)	4.6(3.6)	5.41	3.1(0.6)	0.7(0.5)	2.46
$N_a-Fe-N_{ax}-C_L$	45.4(2.0)	45.2(0.3)	0.20	41.1(0.7)	40.9(0.5)	0.20
$N_b-Fe-N_{ax}-C_L$	44.8(1.9)	44.8(0.5)	0.00	47.6(0.7)	48.4(0.5)	−0.80
$C_a-N_a-C_a-C_b$	1.3(0.2)	1.0(0.1)	0.27	2.4(0.0)	0.5(0.1)	1.85
$C_a-N_b-C_a-C_b$	1.1(0.7)	1.0(0.4)	0.11	0.7(0.5)	0.3(0.2)	0.32
$C_a-N_a-C_a-C_m$	170.0(0.7)	175.3(0.1)	−5.27	176.6(0.1)	178.8(0.1)	−2.19
$C_a-N_b-C_a-C_m$	169.9(1.9)	175.4(0.9)	−5.43	176.8(1.3)	178.9(0.3)	−2.09
$N_a-C_a-C_b-C_b$	3.4(0.5)	2.7(0.1)	0.73	1.5(0.1)	0.3(0.1)	1.17
$N_b-C_a-C_b-C_b$	2.9(0.5)	2.6(0.3)	0.26	1.8(0.3)	0.3(0.2)	1.57
$C_m-C_a-C_b-C_b$	167.9(1.3)	173.6(0.5)	−5.65	176.6(1.2)	179.0(0.3)	−2.43
$C_a-C_b-C_b-C_a$	3.8(0.6)	3.2(0.1)	0.57	1.1(1.0)	0.2(0.1)	0.90
$N_a-C_a-C_m-C_a$	11.0(2.0)	17.2(0.3)	−6.17	6.4(1.0)	1.1(0.9)	5.30
$N_b-C_a-C_m-C_a$	10.9(2.1)	17.2(2.1)	−6.29	1.4(0.7)	0.9(0.6)	0.48
$C_b-C_a-C_m-C_a$	158.7(1.8)	158.5(1.9)	0.26	175.3(0.9)	179.1(0.4)	−3.83
$C_b-C_a-C_m-C_p$	16.4(3.0)	13.6(1.5)	2.75	6.5(1.5)	3.8(2.9)	2.68
$C_a-C_m-C_p-C_p$	90.0(4.7)	90.0(4.1)	0.00	90.0(12.5)	90.0(2.2)	0.00
$C_p-C_p-C_p-C_p$	0.8(0.5)	0.2(0.1)	0.57	1.1(0.6)	0.1(0.1)	0.96
$C_m-C_p-C_p-C_p$	177.5(1.5)	180.0(0.1)	−2.50	177.5(2.3)	179.7(0.1)	−2.24
$Fe-N_{ax}-C_L-C_L$	1.6(1.2)	0.3(0.1)	1.30	1.4(0.1)	0.3(0.1)	1.10
$Fe-N_{ax}-C_L-N_L$	178.4(0.9)	179.7(0.1)	−1.31	178.5(0.0)	179.7(0.1)	−1.23

Table 6 (Continued)

(C) Torsional Angles (deg)

	[Fe(TMP)(1,2-Me$_2$Im)$_2$]$^+$			[Fe(TMP)(1-MeIm)$_2$]$^+$		
torsions	obs[b]	calc	diff	obs[c]	calc	diff
N_{ax}–Fe–N_a–C_a	68.2(4.7)	71.6(3.5)	−3.40	90.0(2.2)	90.0(1.3)	0.00
C_L–N_L–C_L–C_L	0.8(0.6)	0.1(0.1)	0.70	1.4(1.1)	0.3(0.3)	1.10

[a] Values in parentheses are the esd's computed as $\{(\sum x^2 - n\bar{x}^2)/(n-1)\}^{1/2}$, where n is the number of bonds or angles of each type (not shown in the table), x is the value of each observation, and $\bar{x}$ is the mean of each set of observations. C_a, C_b, and C_m are the α, β, and *meso* carbons of the porphyrin, respectively, while C_p and C_L are the carbon atoms in the phenyl groups and axial ligands, respectively. N_a and N_b refer to cis porphyrin nitrogen atoms, while N_{ax} is the bound donor atom of an axial ligand whose nitrogens are otherwise labeled N_L. [b] This work. [c] Reference 21.

Parts a and b of Figure 5 show the procedure in more graphic detail for the hypothetical low-spin [Fe(TMP)]$^+$ complex. Two dihedral angles χ_1 and χ_3, describing the orientations of an opposite pair of *meso*-mesityl groups, are selected as the reaction coordinate for the grid search. Both dihedral angles are then counterrotated through an angle range of 40−140° in 5° increments. This produces 400 conformations or grid points; the geometry of each conformation is optimized by energy minimization prior to proceeding to the next point. The total strain energy or change in strain energy (ΔU_T, Figure 5b) is then plotted as a function of the reaction coordinate to generate the energy surface. Figure 5a shows three structures selected from the diagonal cross-section through the strain energy surface in Figure 5b. Also shown are the energies,[74a] coordination sphere geometries, and core conformations of the three conformers. From Figure 5a, the planar conformation is lowest in energy and exhibits near-perfect D_{4h} symmetry with equivalent Fe−N_p distances of 1.981 Å and negligible displacements of the core atoms from the mean plane of the metalloporphyrin. In contrast, the distorted conformer at the coordinate χ_1, χ_3 = 50° is 7.18 kcal/mol higher in energy than the global minimum conformation (χ_1, $\chi_3 \approx 90°$) and, because it is slightly more ruffled, somewhat higher in energy than the distorted conformer at χ_1, χ_3 = 130°.[74b]

The distorted conformers exhibit perfect D_{2d} symmetry, as reflected by the perpendicular displacements of the core atoms from the mean plane of the metalloporphyrin and the two pairs of inequivalent Fe−N_p distances. An important observation is that the calculated D_{2d}-symmetry distortion of the macrocycle is accompanied by contraction of the porphyrin core; the mean Fe−N_p distance shortens by 0.008 Å in going from the minimum-energy planar conformation to either of the nonplanar D_{2d} conformations. One reason for this is that the distorted conformers in Figure 5a are a mix between an ideal D_{2d}-*ruf* and an ideal D_{2d}-*sad* geometry, since not only are the pyrrole β-carbon pairs alternately displaced above and below the mean molecular plane (normal *sad*[39,40] conformation) but so too are the *meso* carbons (normal *ruf*[39,40] conformation). Since a *ruf* distortion allows rotation of the pyrrole rings about the Fe−N_p bonds, which then shorten significantly, the presence of this type of symmetry element in the calculated nonplanar conformations probably accounts for much of the observed core contraction.

Diagonal cross-sections through the strain energy surfaces for [Fe(TPP)]$^+$, [Fe(T-2,6-Cl_2PP)]$^+$, and [Fe(TMP)]$^+$ are shown in Figure 5c. The change in total steric energy with dihedral angle to the opposite *meso* substituents clearly depends on the size of the rotated aryl groups and follows the order phenyl ≪ 2,6-dichlorophenyl < mesityl. This order is consistent with a sterically-driven change in core conformation brought about by rotation of the *meso*-aryl groups. Interestingly, the steric bulk of the 2,6-dichlorophenyl group is almost equivalent to that of the mesityl group (cf. Figure 5c); this means that four-coordinate and axially ligated complexes of [Fe(T-2,6-Cl_2PP)]$^+$ should be nearly isostructural with those of [Fe(TMP)]$^+$.

We[40] have suggested that *sad* conformations are induced by lattice interactions that tip the phenyl groups toward the porphyrin core in [M(TPP)]$^{n+}$ complexes. The present, and our previous,[41] calculations confirm this mechanism since the minimum energy orientations of the *meso*-aryl substituents (Figure 5a−c) are at about 90°, while any orientation other than 90° represents the effect of an extramolecular perturbation to the conformation of the substituent groups. The conformations of the peripheral *meso* substituents may, however, depend on the disposition of nonbonded contacts within an axially ligated complex (*vide infra*). An important point, which will become apparent in the following discussion for the *six-coordinate ruf* conformers of [Fe(TMP)]$^+$ (axially ligated by sterically hindered imidazoles and pyridines), is that the axial ligand−porphyrin core interaction is dominant, and that rotation of the *meso*-aryl substituents cannot seriously perturb the core geometry from the D_{2d}-*ruf* symmetry imposed by the axial ligands.

***D*$_{2d}$-*ruf* [Fe(TMP)(L)$_2$]$^+$ Complexes: The Effect of Axial Ligand and Peripheral Group−Porphyrin Interactions on the Molecular Conformation.** The fundamental objective of the following MM calculations was to explore the collective influence of nonbonded interactions between a series of axial ligands of increasing steric bulk, the peripheral mesityl groups, and the porphyrin core on the overall molecular conformation in *six-coordinate* iron(III) complexes of TMP. Conformational mapping experiments were performed by counterrotation of an opposite pair of mesityl groups in 5° increments in the range 40−140°, as described above, on [Fe(TMP)(4(5)-MeHIm)$_2$]$^+$, [Fe(TMP)(Py)$_2$]$^+$, [Fe(TMP)(1,2-Me$_2$Im)$_2$]$^+$, [Fe(TMP)(BzHIm)$_2$]$^+$, and [Fe(TMP)(2-MeBzHIm)$_2$]$^+$.

Figure 6a shows a plot of the *change* in total strain energy for [Fe(TMP)(1,2-Me$_2$Im)$_2$]$^+$ as a function of the orientations (χ_1 and χ_3) of an opposite pair of mesityl groups, while the analogous surface for the low-spin D_{2d}-*ruf* [Fe(TMP)(2-MeBzHIm)$_2$]$^+$ complex is given in Figure 6b. (These two strain energy surfaces were chosen for illustration.) In contrast to the

(73) The global energy minimum corresponds to a planar D_{4h} core conformation with *meso*-aryl orientations close to 90° relative to the flanking pyrrole rings of the porphyrin.[41] However, rotational deformation of the peripheral aryl groups, a phenomenon known to occur in the crystalline state,[40] is capable of driving conversion of the planar core conformer into one exhibiting a *saddle* distortion with D_{2d} symmetry. Tipping over the substituents attached to the *meso* carbons of the metalloporphyrin forces an increase in nonbonded repulsion between each substituent and the adjacent pyrrole rings of the porphyrin, which then propagates the rotational deformation of torsion angles in the macrocycle.[41]

(74) (a) The energy value given is that relative to the global minimum conformation. (b) Only two dihedral angles (χ_1 and χ_3) are restricted during conformational mapping; all others are allowed to refine freely. The dihedral angles describing the orientations of the other two *meso*-aryl groups, χ_2 and χ_4, therefore exhibit values closer to 90°, which is the ideal (strain-free) orientation in an *undistorted* conformation. Using Figure 5a for illustration, specific values of the mesityl group orientations are: χ_1, χ_3 = 50.0°, χ_2, χ_4 = 85.5°; χ_1, χ_3 = 90.0°, χ_2, χ_4 = 90.0°; and χ_1, χ_3 = 130.0°, χ_2, χ_4 = 85.7°.

(a)

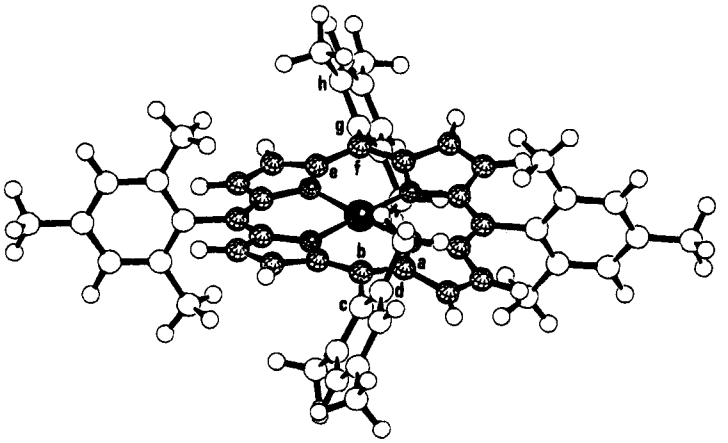

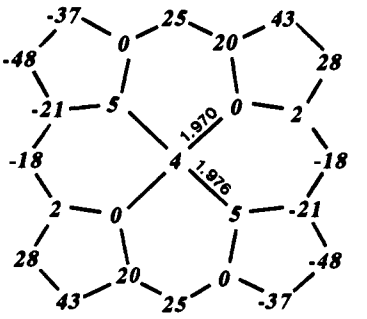

ΔU_T = 7.18 kcal.mol^{-1} χ_1 = a–b–c–d = 50°
χ_3 = e–f–g–h = 50°

D_{2d}-*sad*

Fe–N_p = 1.973(3) Å

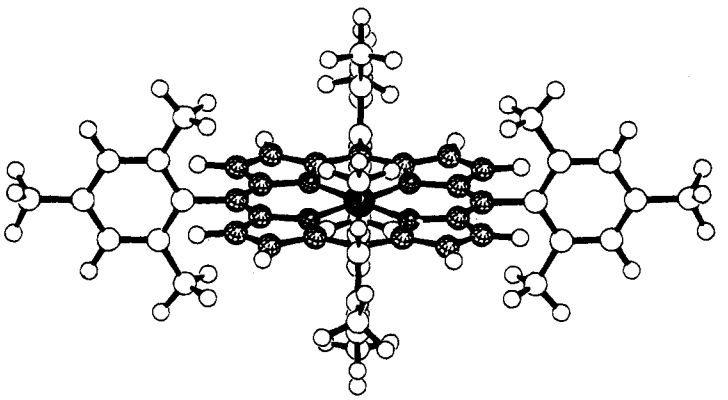

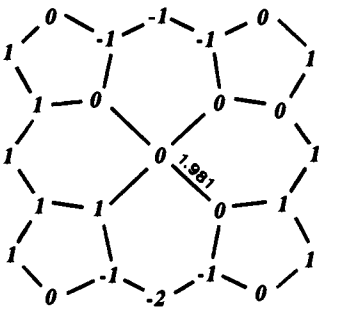

ΔU_T = 0.00 kcal.mol^{-1} χ_1 = 90°
χ_3 = 90°

~planar (D_{4h})

Fe–N_p = 1.981(0) Å

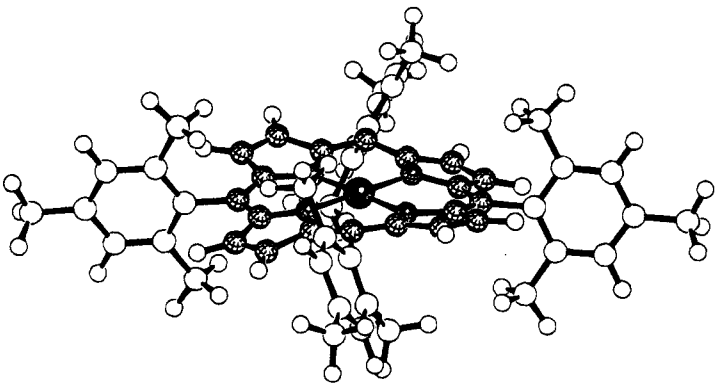

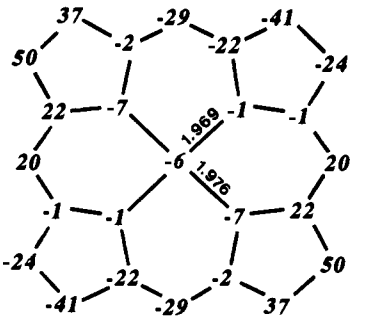

ΔU_T = 6.80 kcal.mol^{-1} χ_1 = 130°
χ_3 = 130°

D_{2d}-*sad*

Fe–N_p = 1.973(4) Å

Figure 5. (a) Selected structurally-refined $[Fe(TMP)]^+$ conformations taken off the diagonal of the strain energy surface shown in part b, along with their relative energies,[74a] core conformations, and coordination sphere geometries. Atom displacements are in units of 0.01 Å and Fe–N_p bond lengths are in Å. The strain energy surface was generated by counterrotating an opposite pair of mesityl group dihedral angles, χ_1 and χ_3, from 40 to 140° in 5° increments, with energy minimization at each incremented grid coordinate.[74b] (c) Variation of the change in total strain energy (ΔU_T, in kcal·mol^{-1}) as a function of *meso*-aryl substituent orientation, χ_i, along the diagonal cross-sections through the strain energy surfaces for $[Fe(TPP)]^+$, $[Fe(T\text{-}2,6\text{-}Cl_2PP)]^+$, and $[Fe(TMP)]^+$.

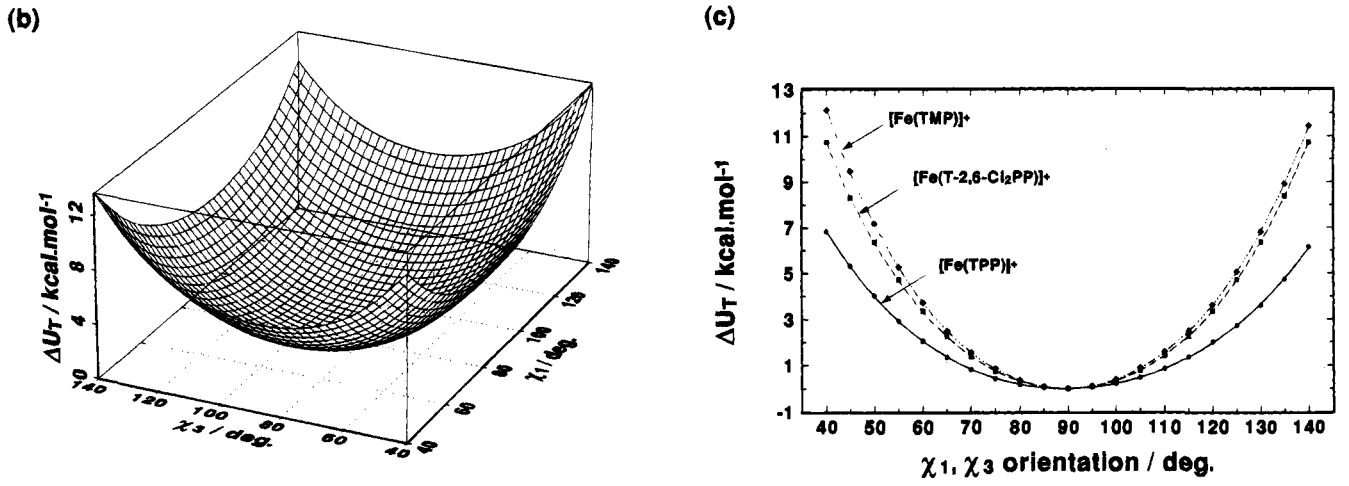

Figure 5. (Continued)

four-coordinate complex $[Fe(TMP)]^+$, the minimum energy conformation is not located at χ_1, $\chi_3 \approx 90°$[75a] in either the bis(1,2-Me_2Im) or the bis(2-MeBzHIm) complex. The minimum energy orientations of the trans mesityl groups in the axially ligated complexes are actually shifted toward χ_1, $\chi_3 \approx$ 85° (opposite mesityl groups staggered when looking down the vector passing through C_m–Fe–C_m). The minimum for the bis-(2-MeBzHIm) complex lies exactly on the diagonal at 84.9°, whereas that for the bis(1,2-Me_2Im) complex lies just off the diagonal with $\chi_1 = 85.0°$ and $\chi_3 = 87.5°$. These results reflect the apportionment of steric bulk in the axial ligands; the interactions between mesityl groups 1 and 3 and the axial ligands are essentially equivalent in $[Fe(TMP)(2\text{-MeBzHIm})_2]^+$, but they are greater between mesityl group 1 and the α-methyl group of 1,2-Me_2Im in $[Fe(TMP)(1,2\text{-}Me_2Im)_2]^+$. The minimum energy orientation for this substituent is therefore lower ($\chi_1 = 85.0°$) than the sterically favored orientation of the opposite mesityl group ($\chi_3 = 87.5°$). The position of the strain energy minimum on this type of perturbation surface therefore reflects the nature and distribution of steric bulk in the axial ligands and confirms the existence of a through-space interaction between the axial ligands and peripheral mesityl substituents.

An interesting feature evident on the strain energy surface for $[Fe(TMP)(2\text{-MeBzHIm})_2]^+$ is the perturbation located in the two regions $\chi_1 < 75°$ and $\chi_1 > 95°$, along $\chi_3 = 65°$ (Figure 6b). The diagonal cross-section through the strain energy surface (not shown) confirms this observation since there is a significant step in complex strain energy when χ_1 and χ_3 rotate through the diagonal coordinate 65°, 65°.

Figure 7 plots the change in core geometry as a function of the counterrotation of opposite mesityl groups in $[Fe(TMP)(2\text{-MeBzHIm})_2]^+$. The data were obtained by fitting least-squares planes through the 25-atom cores of the refined structures lying along the diagonal in Figure 6b. From Figure 7, the origin of the step in the strain energy perturbation surface is clearly identified as a marked increase in the extent of distortion of the porphyrin core at χ_1, $\chi_3 = 65°$. Our previous calculations[41] on $[Fe(TPP)]^+$ indicated that such structural reorganization

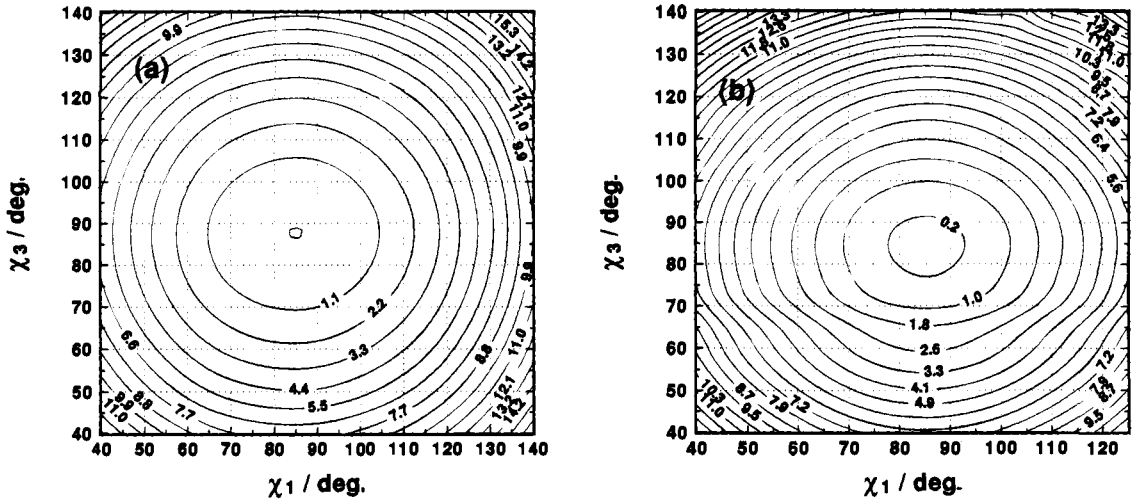

Figure 6. (a) Map of the change in total strain energy (ΔU_T, in kcal·mol^{-1}) as a function of the counterrotation of trans mesityl groups in $[Fe(TMP)(1,2\text{-}Me_2Im)_2]^+$. The minimum in the strain energy surface lies at $\chi_1 \sim 85.0°$ and $\chi_3 \sim 87.5°$, while the minimum obtained from a 4th order polynomial fit of the diagonal cross-section is 86.1°. The global minimum conformation exhibits a strong ligand-induced D_{2d}-*ruf* core geometry, with minimum-energy mesityl group orientations tilted from the heme normal (χ_1, $\chi_3 \neq 90°$) due to nonbonded interactions with the coordinated ligands. The unperturbed strain energy surface maps the global minimum region of conformational space and exhibits no saddle points characteristic of conformational interconversion. (b) Map of the change in total strain energy (ΔU_T, in kcal·mol^{-1}) obtained as a function of the counterrotation of trans mesityl groups in $[Fe(TMP)(2\text{-MeBzHIm})_2]^+$. The strain energy minimum is located on the diagonal cross-section at χ_1, $\chi_3 = 84.9°$. The surface shows significant perturbations in the two regions $\chi_1 < 75°$ and $\chi_1 > 95°$, along $\chi_3 = 65°$. The origin of these features is discussed in the text. The strain energy surfaces were generated as before (Figure 5) by counterrotating an opposite pair of mesityl group dihedral angles, χ_1 and χ_3, from 40 to 140° in 5° increments; energy minimization was effected at each incremented grid coordinate.

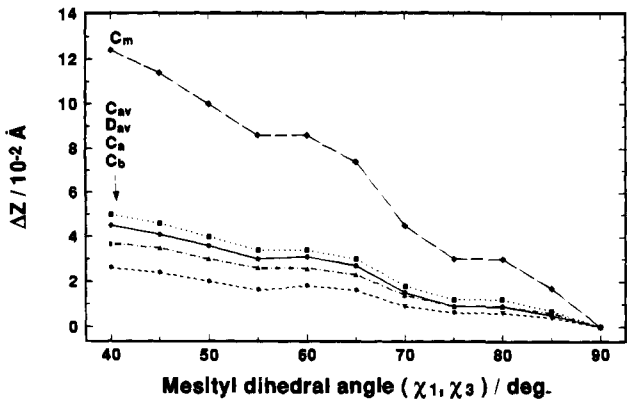

Figure 7. Plot of the parameters demarcating the extent of porphyrin core ruffling accompanying the counterrotation of trans mesityl groups in $[Fe(TMP)(2\text{-}MeBzHIm)_2]^+$. ΔZ is the general label for the *change*, relative to the conformation at $\chi_1, \chi_3 = 90°$, in the mean absolute perpendicular displacements of the different classes of core atoms from the mean plane through the metalloporphyrin. C_a, C_b, and C_m refer to the α, β, and *meso* carbons, respectively; C_{av} is the average for all the carbon atoms, while D_{av} is the average for all the core atoms including the metal ion.

occurred only at staggered phenyl dihedral angles of 55°. In the present case, strong S_4 ruffling of the porphyrin core, brought about by the staggered orientation of the axial 2-MeBzHIm ligands, coupled with the larger steric bulk of the *meso* substituents, enhances the nonbonded interaction between the rotating mesityl groups and the porphyrin ring to bring about conformational reorganization at 65°. The identity of the axial ligands is important in this mechanism because the strain energy surfaces for the other $[Fe(TMP)(L)_2]^+$ complexes are, in contrast, unperturbed. The bis(2-MeBzHIm) complex of $[Fe(TMP)]^+$ actually has the most ruffled calculated core geometry in this series, with $C_m = 0.81$ Å, $C_b = 0.28$ Å, $C_a = 0.43$ Å, $C_{av} = 0.45$ Å, and $D_{av} = 0.36$ Å for the minimum energy conformer ($\chi_1, \chi_3 = 85°$, staggered trans mesityl groups).[75b] This extreme distortion of the porphyrin core in fact restricted the scan of conformational space (Figure 6b) to the χ_1 range of 40° to 125°; at higher values of χ_1, structural refinement failed to converge to within the set limit and the search was necessarily abandoned.

Unambiguous evidence to support the proposal that the axial ligand−porphyrin core nonbonded interaction is the primary determinant of core conformation in *six-coordinate* metalloporphyrin species may be obtained from the strain energy maps generated by the systematic grid search method. One can look at selected refined structures and strain energy profiles from either the diagonal cross-section through the energy surface or some other cross-section. We found that cross-sections along the line described by $\chi_3 = 50°$ and $\chi_1 = 40-140°$ (cf. Figure 6, part a or b) through the calculated energy surfaces for $[Fe(TMP)(Py)_2]^+$, $[Fe(TMP)(1,2\text{-}Me_2Im)_2]^+$, $[Fe(TMP)(BzHIm)_2]^+$, and $[Fe(TMP)(2\text{-}MeBzHIm)_2]^+$ resulted in maximal differentiation of the strain energy curves for the four complexes. (Those curves representing the diagonal cross-sections were less distinct owing to exact overlap for $[Fe(TMP)(1,2\text{-}Me_2Im)_2]^+$ and $[Fe(TMP)(BzHIm)_2]^+$.) Figure 8a shows three selected refined structures from Figure 6a along the $\chi_3 = 50°$ cut through the surface. Also shown are the coordination sphere parameters, strain energies,[74a] and core conformations at the selected grid points.[75c] The conformer with $\chi_1, \chi_3 = 85°, 50°$ is lowest in strain along this cut through the surface, but it is *not* the global minimum, which from Figure 6a has mesityl orientations $\chi_1 = 85.0°$ and $\chi_3 = 87.5°$. Torsional angle deformation and through-space van der Waals repulsions are the principal components of the strain energy that lead to the variation shown in Figure 8a. Depending on the orientations of the mesityl groups, and therefore the exact nature of the distortion from ideal D_{2d}-*ruf* symmetry, there are variations in the Fe−N_p bond distances and, to a lesser extent, the Fe−N_{ax} distances. In accord with the behavior of the four-coordinate complexes (*vide supra*), the most strongly ruffled core ($\chi_1, \chi_3 = 140°, 50°$) exhibits the shortest Fe−N_p distances. Thus, although the ligand-induced D_{2d}-*ruf* core geometry promotes a large contraction of the Fe−N_p bonds (relative to the typical distance for planar low-spin iron(III) porphyrins, Fe−N_p ~ 1.990 Å[37]), the magnitude of this contraction is quite clearly modulated by the orientations of the peripheral aryl groups.

The effect of the identity of the axial ligands on the strain energy response surfaces, keeping the type of porphyrin ligand constant throughout (TMP), is shown in Figure 8b.[76] This cut through the surface along $\chi_3 = 50°$ demonstrates that the changes in strain energy arising from distortion of the porphyrin core as the *meso* substituent (χ_1) is rotated from 40° to 140° depend nominally on the size of the coordinated axial ligands. Evidently, the greater the ligand bulk, the greater the D_{2d}-*ruf* distortion of the porphyrin macrocycle, and the greater the magnitude of the nonbonded interactions between the rotating mesityl group(s) and the flanking porphyrin pyrrole rings. (The sides of the strain energy well for $[Fe(TMP)(BzHIm)_2]^+$, for example, are steeper than those for $[Fe(TMP)(Py)_2]^+$.) Although rather modest, the order for the observed effect is pyridine < 1,2-Me_2Im < BzHIm < 2-MeBzHIm.

This attenuated response to rotation of the mesityl groups in these six-coordinate complexes undoubtedly reflects the dominance of the axial ligand−porphyrin interaction in determining the symmetry of the core conformation, which, when locked, is little perturbed by peripheral group effects. This has profound consequences when the crystallization process leads to selection of a thermodynamically unstable rotamer. Two good examples are the crystal structures of $[Fe(OEP)(2\text{-}MeHIm)_2]^+$ [77] and $[Fe(TPP)(BzHIm)_2]^+$,[78] where the axial ligand planes are oriented so that $\phi_1, \phi_2 \approx 22°$ and $\Delta\phi = 0°$, i.e., the axial ligands adopt an *eclipsed* rather than staggered orientation. The disposition of nonbonded contacts between the axial ligands and the porphyrin core when $\Delta\phi = 0°$ results in a planar core geometry for the macrocycle. One consequence is that the ligand−porphyrin nonbonded interactions are lessened by elongation of the Fe−N_{ax} bonds, which reduces the total ligand field strength at the metal ion and thus favors an $S = 5/2$ state. Another example is the monoclinic crystal form of $[Fe(OEP)(3\text{-}ClPy)_2]^+$ [79] where $\phi_1, \phi_2 \approx 10°$ and $\Delta\phi \approx 0°$ and an $S = 3/2$

(75) (a) The dihedral angles measuring the orientation of the *meso*-aryl substituents are given the symbol χ_i to distinguish them from the angles gauging the orientations of the axial ligands (ϕ). A further illustration of this dihedral angle, other than that already given in Figure 5a, would be that involving the atom sequence 47−48−49−49 in Figure 11. (b) Note that these core parameters differ to those displayed in Figure 7, which plots the *change* in each parameter relative to these data for the lowest energy conformation. (c) The dihedral angles defining the orientations of mesityl groups 2 and 4, χ_2 and χ_4, are not restricted during geometry optimization and adopt values closer to the strain-free value of 90°. In Figure 8a, $\chi_1, \chi_3 = 40°, 50°$ with $\chi_2, \chi_4 = 85.6°, 88.0°$; $\chi_1, \chi_3 = 85°, 50°$ with $\chi_2, \chi_4 = 87.2°$; and $\chi_1, \chi_3 = 140°, 50°$ with $\chi_2, \chi_4 = 86.4°$.

(76) In Figure 8b, the energy curves pass through a point near $\chi_1 \sim 85°$ because, in all cases, orientations close to this value correspond to the lowest strain arrangement for the peripheral mesityl substituents.

(77) Geiger, D. K.; Lee, Y. J.; Scheidt, W. R. *J. Am. Chem. Soc.* **1983**, *105*, 2625.

(78) Levan, K. R.; Strouse, C. E. *Abstracts of Papers*, American Crystallographic Association Summer Meeting, Snowmass, CO, Aug 1−5, 1983; Abstract H1. Levan, K. R. Ph.D. Thesis, UCLA, 1984.

(79) Scheidt, W. R.; Geiger, D. K.; Hayes, R. G.; Lang, G. *J. Am. Chem. Soc.* **1983**, *105*, 2625.

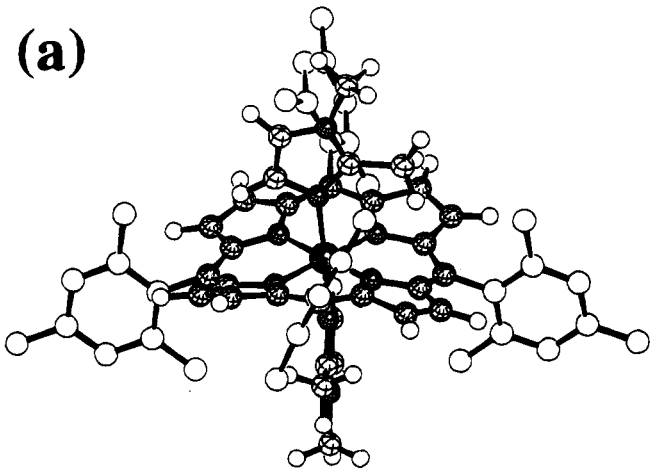

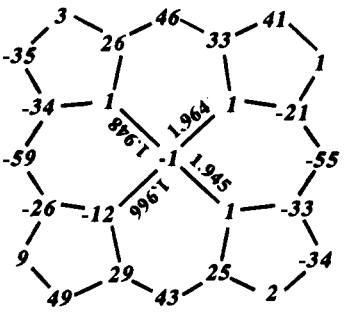

distorted D_{2d}-*ruf*

Fe–N_p = 1.956(11) Å
Fe–N_{ax} = 2.014(0) Å

ΔU_T = 10.63 kcal.mol^{-1}

χ_1 = 40°
χ_3 = 50°

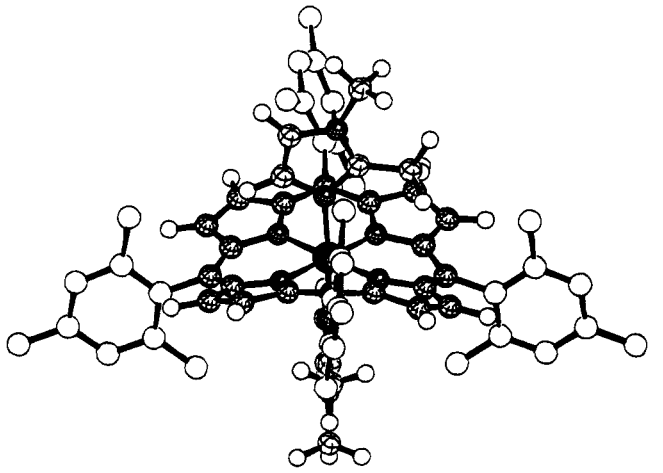

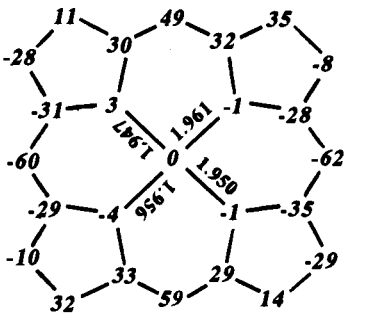

distorted D_{2d}-*ruf*

Fe–N_p = 1.953(6) Å
Fe–N_{ax} = 2.011(0) Å

ΔU_T = 4.43 kcal.mol^{-1}

χ_1 = 85°
χ_3 = 50°

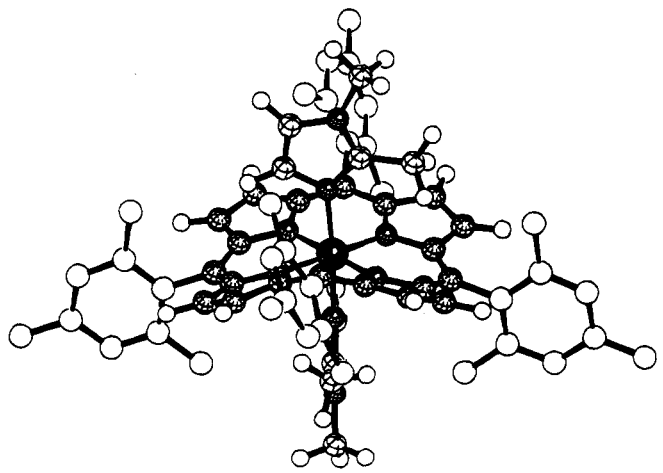

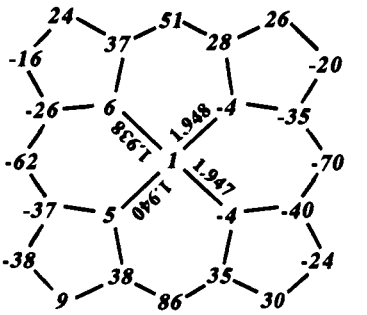

distorted D_{2d}-*ruf*

Fe–N_p = 1.943(5) Å
Fe–N_{ax} = 2.012(3) Å

ΔU_T = 14.56 kcal.mol^{-1}

χ_1 = 140°
χ_3 = 50°

Figure 8. (a) Three selected structurally-refined $[Fe(TMP)(1,2\text{-}Me_2Im)_2]^+$ conformations taken from the strain energy surface shown in Figure 6a, with grid coordinates (trans mesityl group orientations) χ_1, χ_3 = 40°, 50°; χ_1, χ_3 = 85°, 50°; and χ_1, χ_3 = 140°, 50°. Strain energies,[74a] core conformations, and coordination sphere geometries are shown. (Atom displacements are in units of 0.01 Å, and Fe–N_p bond distances are in Å.) Mesityl group hydrogen atoms have been omitted for clarity.

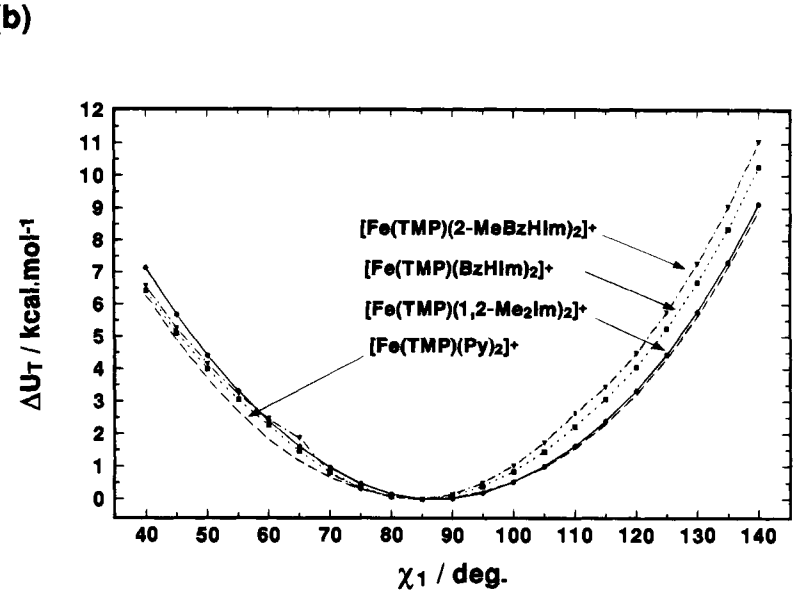

Figure 8. (b) Plot of the change in total strain energy (ΔU_T, in kcal·mol^{-1}) for four highly ruffled six-coordinate low-spin complexes of iron(III) TMP as a function of the rotation of mesityl group 1 (χ_1), at a fixed mesityl group 3 orientation ($\chi_3 = 50°$). The dependence of the strain energy surface cross-sections on axial ligand identity is attenuated by the strong ligand-induced D_{2d} ruffling of the porphinato cores in each case. The perturbations seen in Figure 6b for the [Fe(TMP)(2-MeBzHIm)$_2$]$^+$ complex are visable at $\chi_1 = 65°$ and 110°.

Table 7. Calculated Minimum Energy (Staggered) Orientations of Trans Mesityl Groups in Several Axially Ligated Low-Spin Iron(III) TMP Complexes, with Corresponding van der Waals Volumes of the Axial Ligands in Each Case

complex	χ_1, $\chi_{3(min)}$, deg	ligand volume (Å^3)
[Fe(TMP)(5-MeHIm)$_2$]$^+$	87.20	56.9[a]
[Fe(TMP)(Py)$_2$]$^+$	86.42	71.4
[Fe(TMP)(1,2-Me$_2$Im)$_2$]$^+$	86.12	88.1
[Fe(TMP)(BzHIm)$_2$]$^+$	85.91	93.9
[Fe(TMP)(2-MeBzHIm)$_2$]$^+$	84.88	110.3

[a] Volume of imidazole; use of the total volume of 5-MeHIm (72.8 Å^3) is incorrect here because the methyl group in 5-MeHIm does not interact with the closest mesityl group of the porphyrin ligand.

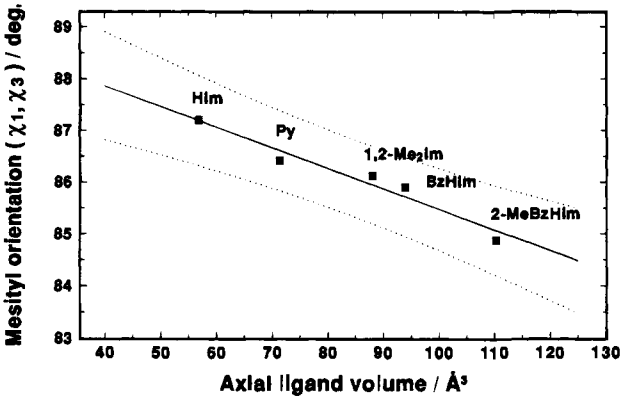

Figure 9. The dependence of the staggered minimum energy orientations of a trans pair of mesityl groups on the van der Waals volumes of the axial ligands in a series of [Fe(TMP)(L)$_2$]$^+$ complexes where the axial ligands, L, are planar imidazoles or pyridines. The 95% confidence interval of the fitted function (f(V) = (89.5 ± 0.5°) − (3.985 ± 0.005) × 10^{-2} V) is shown.

state ensues. The orientations (ϕ) and relative orientations ($\Delta\phi$) of axial pyridine or imidazole ligands in iron(III) porphyrins may therefore determine the spin state of the metal, and it follows that there can exist a critical temperature range in solution[27] where both limiting rotamers ($\Delta\phi \approx 90°$ and $\Delta\phi \approx 0°$) are populated according to a Boltzmann distribution determined by the energy difference between the high-spin (planar) and low-spin (ruffled) conformational states.

Computational Evidence for Nonbonded Interactions between Coordinated Axial Ligands and Peripheral Mesityl Substituents. The diagonal cross-sections through the strain energy response surfaces for [Fe(TMP)(4(5)-MeHIm)$_2$]$^+$, [Fe(TMP)(Py)$_2$]$^+$, [Fe(TMP)(1,2-Me$_2$Im)$_2$]$^+$, [Fe(TMP)(BzHIm)$_2$]$^+$, and [Fe(TMP)(2-MeBzHIm)$_2$]$^+$ were fitted to 4th order polynomials and the turning points determined by differentiation (Table 7). The minimum energy orientations of the staggered mesityl groups depend on the identity of the axial ligands, moving away from the coordinate $\chi_1, \chi_3 = 90°$ as the size of the axial ligands increases from (4)5-MeHIm to 2-MeBzHIm. The relationship plotted in Figure 9 is linear (f(V) = (89.5 ± 0.5°) − (3.985 ± 0.005) × 10^{-2} V, $R^2 = 0.95$, esd = 0.22), with the intercept of the fitted function predicting a lowest energy orientation for the *meso*-mesityl groups in a four-coordinate TMP complex of 89.5 ± 0.5°. Since the mean minimum energy orientation of the peripheral aryl groups of the four-coordinate complexes in Figure 5c is 89.7 ± 0.3°, the correlation between mesityl group orientation and axial ligand size seems to be reliable for such predictions. More significantly, however, Figure 9 demonstrates for the first time that the axial ligands influence the orientations of the peripheral substituents in such complexes.[80]

Recent interest in the rotational dynamics of axial ligands in iron(III) tetraarylporphyrins[26-28,81] has sought to determine the preferred relative orientations, as well as orientations relative to the porphyrin core, of several sterically hindered imidazoles using ^{1}H NMR spectroscopy. Walker and Simonis[26] demonstrated that at low temperatures the favored orientation of the 2-MeHIm ligands in [Fe(TMP)(2-MeHIm)$_2$]$^+$ places the staggered ligand planes over the *meso* carbon atoms of the porphyrin

(80) It should be noted that the van der Waals volume of imidazole and *not* 5-MeHIm was used in Figure 9; the reason for this is that the methyl group attached to C_5 in 5-MeHIm does not interact significantly with the closest mesityl group of the porphyrin, and may therefore be considered to contribute negligible contact volume to the interaction. This may be confirmed from inspection of a space-filling plot of the refined molecular structure of [Fe(TMP)(5-MeHIm)$_2$]$^+$.

(81) Nakamura, M.; Groves, J. T. *Tetrahedron* **1988**, *44*, 3225.

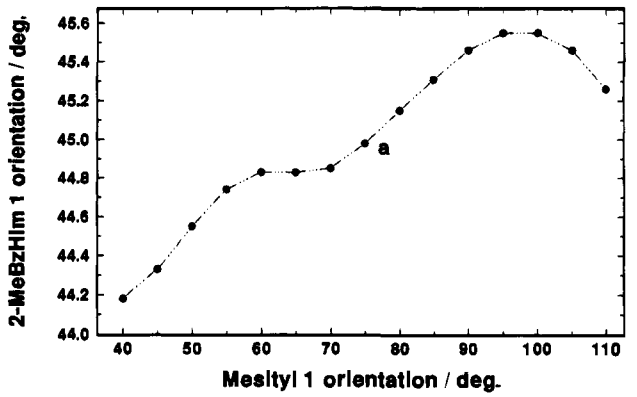

Figure 10. Variation of the axial ligand orientation (ϕ) with the changing orientation of the closest mesityl group (χ_1) for the counter-rotation of trans mesityl groups in D_{2d}-ruffled [Fe(TMP)(2-MeBzHIm)$_2$]$^+$. Rotation of the mesityl groups effects a change in core geometry, with a consequent change in the ligand orientation, until direct perturbation of the axial ligand orientation due to the mesityl–ligand through-space interaction sets in. The observed ligand–peripheral group interaction confirms the previous suggestions of Scheidt and co-workers[21] regarding the likely mechanism of *enhancement* of S_4 ruffling in axially ligated low-spin iron(III) TMP complexes.

core, in accord with X-ray studies on such systems.[21,42] At higher temperatures, however, rotation of the axial ligands drove interconversion of the porphyrin macrocycle between S_4-ruffled enantiomers, as characterized by an alternate up-down (wagging) motion of the pairs of trans mesityl groups relative to the mean porphyrin plane. This motion of the mesityl groups arises from the changes in porphyrin core geometry effected by rotation of the axial ligands. Although probably difficult to detect experimentally, we wondered whether thermal libration of the mesityl groups in such a complex could perturb the orientations of the axial ligands, perhaps as a result of the through-space interaction between the closely juxtaposed groups.

Figure 10 traces the dependence of the orientation of one axial ligand on the orientation of the closest *meso*-mesityl group in [Fe(TMP)(2-MeBzHIm)$_2$]$^+$ (from the diagonal cross-section through the strain energy response surface in Figure 6b). When $40° < \chi_1 < 60°$, the porphyrin core is strongly distorted, but progressively relaxes into a more regular D_{2d} conformation as the mesityl group is rotated upwards; the ligand-induced pocket in the porphyrin core effectively migrates toward the bisector of a N_a–Fe–N_b angle (equivalent to $\phi = 45°$). Because the axial ligand "follows" the migrating trough in the porphyrin core, it gradually approaches the sterically favored orientation of $\phi = 45°$, which is reached when $\chi_1 = 75°$ (point **a** in Figure 10). As χ_1 pushes on toward 90°, however, the ligand is deflected (as a consequence of the through-space interaction with the mesityl group) to an orientation beyond $\phi = 45°$. The maximum in Figure 10 occurs when χ_1 is ~10° beyond the heme normal. Since the rotating mesityl group no longer interacts strongly with the coordinated ligand beyond $\chi_1 \sim 100°$, the ligand tracks back toward the sterically favored orientation ($\phi = 45°$).

These results suggest that when the peripheral *meso*-aryl substituents and the planar axial ligands are of sufficient steric bulk, the thermal motion of one may appreciably influence that of the other. A noteworthy caveat here is that this conclusion is somewhat limited by the fact that the calculations are not truly dynamic and seek to describe a phenomenon that might be better analyzed using molecular dynamics,[82] which would certainly uncover any motional correlation between the rotatable groups over time. Finally, it should be noted that since both the changing porphyrin core geometry and the mesityl group–

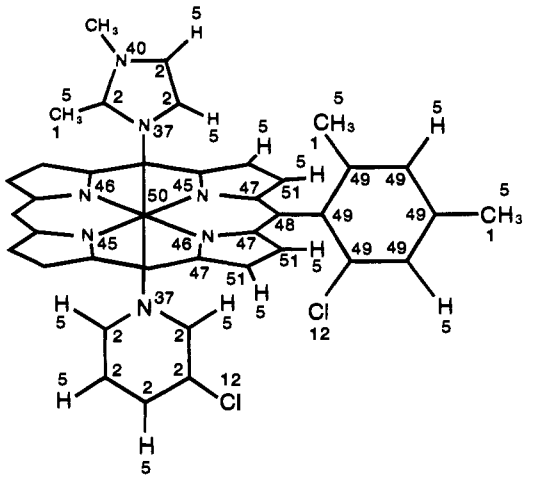

Figure 11. Diagram depicting the atom number types for specifying bond lengths, bond angles, torsion angles, and other interactions in the force field. Two types of porphyrin nitrogen have been defined to allow "pseudo"-torsion angle parameters such as 45–50–45–47 to be set to zero, while permitting parametrization of torsion angles such as 46–50–45–47. Standard MM2[43] atom types have numbers ≤40.

axial ligand nonbonded interaction influence the ligand orientation ϕ, it is not a simple function of χ.

Conclusions

Using a newly derived molecular mechanics (MM) force field for iron(III) porphyrins with a modified version of the program MM2(87), we have been able to accurately model the available ruffled and planar low-spin pyridine and imidazole complexes of [Fe(TMP)]$^+$, including the observed dependence of the Fe–N_p distances on the extent of S_4 ruffling of the porphyrin core. The present X-ray structure analysis of [Fe(TMP)(1,2-Me$_2$-Im)$_2$]$^+$, in conjunction with the MM calculations, indicates that the geometry of the porphyrin core depends on the staggered orientation of the axial imidazole ligands, as well as the axial (above-plane) distribution of steric bulk in contact with the porphyrin macrocycle. The Mössbauer parameters for the complex at 120 and 250 K confirm a relative perpendicular orientation for the axial ligands.

Conformational mapping experiments with [Fe(TPP)]$^+$, [Fe(T-2,6-Cl$_2$PP)]$^+$, and [Fe(TMP)]$^+$ demonstrate that the size of the *meso*-aryl groups determines the extent of *sad* ruffling of the porphyrin core, which increases with increasing steric bulk of the substituents: phenyl ≪ 2,6-dichlorophenyl < mesityl. Analogous experiments with D_{2d}-*ruf* [Fe(TMP)(L)$_2$]$^+$ complexes, where L = pyridine, (4)5-MeHIm, 1,2-Me$_2$Im, BzHIm, and 2-MeBzHIm, show that axial ligand–peripheral group nonbonded interactions play a key role in fine-tuning the conformations of these complexes. The minimum energy orientations of the mesityl substituents, for example, exhibit a linear dependence on the van der Waals volume of the axial ligands, decreasing with increasing ligand size. Moreover, for moderate D_{2d}-*ruf* distortions of the porphyrin core, effected by a staggered orientation of the planar axial ligands, rotation of the peripheral groups does not dramatically perturb the porphyrin conformation, indicating that the axial ligand–porphyrin non-

(82) In our opinion, a molecular dynamics (MD) simulation of this phenomenon would require that "snapshots" of conformations be collected at set times during the dynamics run at a temperature high enough to bring about thermal libration of the *meso*-aryl groups. Values of χ and ϕ would have to be measured for an ensemble of say 100–200 of these snapshot conformations and then plotted against each other to search for a possible correlation.

Table 8. New Parameters for Low-Spin Bisimidazole and Bispyridine Complexes of Highly-Ruffled Iron(III) Porphyrins[a]

(A) Torsional Parameters[b] (kcal·mol^{-1})

atom I	atom J	atom K	atom L	V_1	V_2	V_3	atom I	atom J	atom K	atom L	V_1	V_2	V_3
Fe(50)	N_{ax}(37)	^{2}C(2)	^{2}C(2)	0.000	12.000	0.000	H(5)	C_b(51)	C_b(51)	H(5)	0.000	10.000	0.000
N(45/46)	Fe(50)	N_{ax}(37)	^{2}C(2)	0.000	0.000	0.000	H(23)	N_L(40)	^{2}C(2)	N_{ax}(37)	0.000	15.000	0.000
N_{ax}(37)	Fe(50)	N(45/46)	C_a(47)	0.000	0.000	0.000	H(23)	N_L(40)	^{2}C(2)	^{2}C(2)	0.750	10.000	0.000
N_{ax}(37)	Fe(50)	N_{ax}(37)	^{2}C(2)	0.000	0.000	0.000	H(23)	N_L(40)	^{2}C(2)	H(5)	0.000	10.000	0.000
N(46)	C_a(47)	C_m(48)	C_p(49)	0.000	2.500	0.000	^{3}C(1)	N_L(40)	^{2}C(2)	^{3}C(1)	0.000	10.000	0.000
C_b(51)	C_b(51)	C_a(47)	N(45/46)	0.000	4.000	0.000	H(5)	^{2}C(2)	N_{ax}(37)	Fe(50)	0.000	12.000	0.000
H(5)	C_b(51)	C_a(47)	N(45/46)	0.000	8.000	0.000	N_L(40)	^{2}C(2)	N_{ax}(37)	Fe(50)	0.000	12.000	0.000
C_a(47)	N(45/46)	C_a(47)	C_b(51)	0.000	14.000	0.000	H(5)	^{3}C(1)	^{2}C(2)	N(37/40)	0.000	0.000	−0.240
H(5)	C_m(48)	C_a(47)	C_b(51)	0.000	2.500	0.000	^{3}C(1)	^{2}C(2)	N_{ax}(37)	Fe(50)	0.000	3.000	0.000
C_b(51)	C_a(47)	N(45/46)	Fe(50)	0.000	0.100	0.000	^{3}C(1)	^{2}C(2)	N(37/40)	^{2}C(2)	0.000	10.000	0.000
C_a(47)	N(45)	Fe(50)	N(46)	0.000	0.100	0.000	^{3}C(1)	^{2}C(2)	N_L(40)	H(23)	0.000	10.000	0.000
C_a(47)	N(46)	Fe(50)	N(45)	0.000	0.100	0.000	H(5)	^{3}C(1)	N_L(40)	^{2}C(2)	0.000	0.000	−0.240
N(45)	C_a(47)	C_m(48)	C_p(49)	0.000	3.000	0.000	^{2}C(2)	^{2}C(2)	N_L(40)	^{3}C(1)	0.000	10.000	0.000
N(45)	C_a(47)	C_m(48)	H(5)	0.000	3.800	0.000	H(5)	^{2}C(2)	N_L(40)	^{3}C(1)	0.000	10.000	0.000
C_a(47)	C_m(48)	C_p(49)	C_p(49)	0.000	0.000	0.000	N_{ax}(37)	^{2}C(2)	N_L(40)	^{3}C(1)	0.000	10.000	0.000
C_b(51)	C_a(47)	C_m(48)	C_p(49)	0.000	1.600	0.000	Cl(12)	C_p(49)	C_p(49)	C_m(48)	0.000	0.000	0.000
C_b(51)	C_a(47)	C_m(48)	H(5)	0.000	2.500	0.000	Cl(12)	C_p(49)	C_p(49)	C_p(49)	0.000	15.000	0.000
C_m(48)	C_a(47)	N(45/46)	Fe(50)	0.000	0.200	0.000	H(5)	C_p(49)	C_p(49)	Cl(12)	0.000	15.000	0.000
N(45/46)	C_a(47)	C_m(48)	C_a(47)	0.000	2.000	0.000	Cl(12)	^{2}C(2)	^{2}C(2)	^{2}C(2)	0.000	3.000	0.000
C_a(47)	C_m(48)	C_a(47)	C_b(51)	−0.170	1.200	0.000	Cl(12)	^{2}C(2)	^{2}C(2)	H(5)	0.000	3.000	0.000
C_a(47)	N(45/46)	C_a(47)	C_m(48)	0.000	8.500	0.000	Cl(12)	^{2}C(2)	^{2}C(2)	N_{ax}(37)	0.000	3.000	0.000
C_m(48)	C_a(47)	C_b(51)	C_b(51)	0.000	2.400	0.000	H(5)	^{3}C(1)	C_p(49)	C_p(49)	0.000	0.000	−0.240
^{3}C(1)	C_b(51)	C_b(51)	C_a(47)	−0.270	9.000	0.000	^{3}C(1)	C_p(49)	C_p(49)	C(48/49)	−0.270	10.000	0.000
H(5)	C_b(51)	C_a(47)	C_m(48)	0.000	7.000	0.000	^{3}C(1)	C_p(49)	C_p(49)	H(5)	0.000	12.000	0.000
H(5)	C_b(51)	C_b(51)	C_a(47)	0.000	3.500	0.000							

(B) Bond Stretching Parameters[c]

atom I	atom K	stretching constant (mdyn·Å^{-1})	min energy bond length (Å)	atom I	atom K	stretching constant (mdyn·Å^{-1})	min energy bond length (Å)
N(45/46)	Fe(50)	1.670	1.922	^{2}C(2)[j]	N_{ax}(37)	11.090	1.375
N_{ax}(37)[d]	Fe(50)	1.580	1.940	^{2}C(2)[h]	^{2}C(2)	9.600	1.350
N_{ax}(37)[e]	Fe(50)	1.580	1.950	^{2}C(2)[i]	^{2}C(2)	9.600	1.385
N_{ax}(37)[f]	Fe(50)	1.900	1.965	^{2}C(2)[j]	^{2}C(2)	9.600	1.395
N_{ax}(37)[g]	Fe(50)	2.700	1.950	^{3}C(1)[h]	N_L(40)	4.500	1.480
^{2}C(2)[h]	N_L(40)	11.090	1.340	^{3}C(1)	C_p(49)	4.400	1.497
^{2}C(2)[j]	N_L(40)	11.090	1.367	Cl(12)	C_p(49)	1.719	1.580
^{2}C(2)[h,i]	N_{ax}(37)	11.090	1.350	^{2}C(2)[h,i]	Cl(12)	2.500	1.723

(C) Angle Bending Parameters[k]

atom I	atom J	atom K	bending constant (mdyn·Å·rad^{-2})	min energy bond angle (deg)	atom I	atom J	atom K	bending constant (mdyn·Å·rad^{-2})	min energy bond angle (deg)
N(45/46)	Fe(50)	N_{ax}(37)	0.300	90.00	H(5)[l]	^{2}C(2)	^{2}C(2)	0.300	127.00
N_{ax}(37)	Fe(50)	N_{ax}(37)	0.200	180.00	H(5)[l]	^{2}C(2)	N_L(40)	0.300	126.00
^{2}C(2)[l]	N_{ax}(37)	Fe(50)	0.300	127.50	H(5)[l]	^{2}C(2)	N_{ax}(37)	0.300	125.00
C_m(48)	C_a(47)	N(45/46)	0.200	125.40	^{2}C(2)[l]	^{2}C(2)	^{2}C(2)	0.430	120.00
Cl(12)	C_p(49)	C_p(49)	0.550	118.80	Fe(50)[m]	N_{ax}(37)	^{2}C(2)	0.300	128.00
N(45/46)	C_a(47)	C_b(51)	0.200	109.90	N_{ax}(37)[m]	^{2}C(2)	N_L(40)	0.430	114.00
N_{ax}(37)[l]	^{2}C(2)	N_L(40)	0.650	111.50	^{2}C(2)[m]	N_{ax}(37)	^{2}C(2)	0.430	104.00
^{2}C(2)[l]	N_L(40)	^{2}C(2)	0.430	107.50	^{2}C(2)[m]	N_L(40)	^{2}C(2)	0.430	107.00
^{2}C(2)[l]	^{2}C(2)	N_L(40)	0.430	107.00	N_L(40)[m]	^{2}C(2)	^{2}C(2)	0.300	118.00
^{2}C(2)[l]	N_{ax}(37)	^{2}C(2)	0.430	105.00	N_{ax}(37)[m]	^{2}C(2)	^{2}C(2)	0.300	120.00
^{2}C(2)[l]	^{2}C(2)	N_{ax}(37)	0.430	109.50	^{2}C(2)[m]	^{2}C(2)	^{2}C(2)	0.430	120.00
H(5)	^{3}C(1)	N_L(40)	0.300	109.50	Fe(50)[n]	N_{ax}(37)	^{2}C(2)	0.300	122.00
^{3}C(1)[l]	N_L(40)	^{2}C(2)	0.400	126.50	^{2}C(2)[n]	N_{ax}(37)	^{2}C(2)	0.430	116.00
^{3}C(1)	^{2}C(2)	N_{ax}(37)	0.450	125.50	N_{ax}(37)[n]	^{2}C(2)	^{2}C(2)	0.430	123.50
^{3}C(1)[l]	^{2}C(2)	N_L(40)	0.380	127.00	^{2}C(2)[n]	^{2}C(2)	^{2}C(2)	0.430	119.00
H(5)	^{3}C(1)	C_p(49)	0.360	109.40	N_{ax}(37)[n]	^{2}C(2)	H(5)	0.300	118.00
^{3}C(1)	C_p(49)	C_p(49)	0.550	121.40	H(5)[n]	^{2}C(2)	^{2}C(2)	0.300	121.00
^{2}C(2)	^{2}C(2)	Cl(12)	0.200	120.00					

[a] For conciseness, the optimized parameters for TMP complexes catalogued here are those which differ from the rudimentary parameters for iron porphyrins that we have developed and wish to address elsewhere.[51b] "Minimum energy" bond lengths and bond angles are sometimes referred to as "strain-free" bond lengths and bond angles. C_a, C_b, C_m, and C_p are labels for the α, β, *meso*, and phenyl carbon atoms of the porphyrin, respectively. N_{ax} is the axial donor nitrogen of the imidazole/pyridine ligand; N_L is the secondary nitrogen of the imidazole ligand; N is the porphinato nitrogen. ^{2}C and ^{3}C designate sp^2- and sp^3-hybridized carbon atoms, respectively. [b] Values refer to the dihedral angle I−J−K−L. V_1, V_2, and V_3 are the 1-, 2-, and 3-fold torsional constants, respectively. [c] Values refer to the bond I−K. [d−g] Metal−ligand compression parameters for imidazoles bearing no substituents attached to C_2,[d] sterically restricted imidazoles such as BzHIm and 2-MeHIm,[e] pyridines bearing no substituents attached to C_2 or C_6,[f] and 4-N-substituted, sterically unhindered pyridines.[g] [h−j] Compression parameters for imidazole,[h] pyridine,[i] and benzimidazole[j] axial ligands. [k] Values refer to the bond angle I−J−K. [l−n] Angle bending constants for axial imidazole,[l] benzimidazole,[m] and pyridine[n] ligands.

bonded interaction is the primary determinant of core conformation in six-coordinate complexes.

Finally, our calculations show that the orientations of the axial ligands may be perturbed by rotation of the peripheral *meso* substituents in six-coordinate low-spin $[Fe(TMP)]^+$ complexes, confirming the existence of axial ligand−mesityl group nonbonded interactions and suggesting that such interactions are important in determining the minimum-energy orientations of the ligands and substituents in the absence of strong extramolecular perturbations.

Acknowledgment. H.M.M. thanks the University of the Witwatersrand, through the Centre for Molecular Design, and the Foundation for Research Development (FRD), Pretoria, for financial support. O.Q.M. thanks AECI Limited and the FRD for postgraduate fellowships. W.R.S. and K.M. thank Dr. Ilona Turowska-Tyrk for data collection assistance and the National Institutes of Health for support of this research at Notre Dame (Grant GM-38401) and for purchase of X-ray instrumentation (Grant RR-06709). P.G.D. thanks the National Institutes of Health for support (GM-16406).

Supplementary Material Available: Table S1, complete crystallographic details, Table S2, anisotropic thermal parameters, Table S3, fixed hydrogen atom positions, Tables S4 and S5, bond distances and bond angles, respectively, for $[Fe(TMP)(1,2\text{-}Me_2Im)_2]ClO_4$, Figure S1, an ORTEP diagram showing hydrogen atom positions (11 pages); listings of observed and calculated structure amplitudes (×10) (38 pages). Ordering information is given on any current masthead page. This material is contained in many libraries on microfiche, immediately follows this article in the microfilm version of the journal, and can be ordered from the ACS; see any current masthead page for ordering information.

JA940499V